ISSN 0016-7029, Geochemistry International, 2008, Vol. 46, No. 7, pp. 637–665. © Pleiades Publishing, Ltd., 2008.
Original Russian Text © B.I. Gongalsky, N.A. Krivolutskaya, A.A. Ariskin, G.S. Nikolaev, 2008, published in Geokhimiya, 2008, No. 7, pp. 691–720.

Inner Structure, Composition, and Genesis of the Chineiskii Anorthosite–Gabbronorite Massif, Northern Transbaikalia

B. I. Gongalsky[a], N. A. Krivolutskaya[b], A. A. Ariskin[b], and G. S. Nikolaev[b]

[a] *Institute of the Geology of Ore Deposits, Petrography, Mineralogy, and Geochemistry, Russian Academy of Sciences, Staromonetnyi per. 35, Moscow, 109017 Russia*
e-mail: gon@igem.ru

[b] *Vernadsky Institute of Geochemistry and Analytical Chemistry, Russian Academy of Sciences, ul. Kosygina 19, Moscow, 119991 Russia*
e-mail: nakriv@mail.ru

Received November 14, 2006

Abstract—The Chineiskii anorthosite–gabbronorite massif is the most typical layered intrusion in Russia, which is accompanied by large V and Cu deposits. This massif is first considered to be a component of the Proterozoic volcanic–plutonic system of the Kodar–Udokan district, whose largest massifs are Chineiskii and Lukturskii. This system also comprises numerous dikes (including the Main gabbronorite dike at the Udokan deposit, whose thickness reaches 200 m), which are likely the magmatic feeders of ancient volcanism. An intermediate position in the vertical section of the magmatic system is occupied by gabbroids, whose exposures occur in the peripheral part of the Lurbunskii granite massif. The intrusive rocks were proved to be genetically interrelated and show certain similar geochemical features: they bear elevated TiO_2 concentrations and have similar trace element patterns and $(La/Sm)_N$ and $(Gd/Yb)_N$ ratios (1.5–2.3 and 1.87–2.06, respectively). The Chineiskii Massif is thought to have been formed by the successive emplacement of genetically similar basic magmas, which produced four rock groups with fine and coarse layering and cyclicity of variable rank (microrhythms, rhythms, units, and series). The results of cluster analysis indicate that the rocks can be classified into 13 petrochemical types. The phase and chemical characteristics of the parental melts of these compositions were simulated with the use of the COMAGMAT-3.5 computer model, which was also applied to evaluate the composition of the most primitive initial magma of the whole Chineiskii Massif. Our results indicate that the primitive magma was heterogeneous (olivine + plagioclase ± titanomagnetite + melt) at a temperature of approximately 1130°C. The initial melt had a ferrobasaltic composition and was close to saturation with magnetite at ~NNO ± 0.5

DOI: 10.1134/S001670290807001X

INTRODUCTION

Interest in layered magmatic complexes is stimulated by their inner structure and related ore mineralization. These complexes first evoked keen interest in the mid-20th century, and this interest reached its peak after the publication of papers by Wager and his colleagues devoted to the Skaergaard Massif [1, 2]. The data obtained on the inner structure of the Bushveld pluton in South Africa, Stillwater in the United States, Great Dike in Zimbabwe, Sudbury, and other massifs with clearly pronounced layering and huge resources of related PGE and Ni ore mineralization notably contributed to progress in petrology and the theory of ore genesis. However, many geological features of these intrusions remain obscure [3–5], and one of the principally important aspects in studying large layered complexes is related to their consideration as marks of ancient plume rock associations [6, 7].

One of such complexes in Russia is the Chinneiskii Massif (Fig. 1), whose inner structure and clearly pronounced layering and cyclicity are comparable to that of the Skaergaard intrusion, and the petrography of the rocks resembles that of the Upper Unit of the Bushveld Massif. Although the sizes of the intrusion are tens of times smaller than those of the aforementioned zone, this intrusion is accompanied by huge resources of V, which are only three times smaller than those at Bushveld. It hosts Russia's largest deposits of Fe–Ti–V ores (the Magnitnoe and Etyrko deposits), which are also among the world's largest [8]. The Chinneiskii Massif is accompanied by deposits of Cu sulfides and precious metals [9–14], which are restricted to the contact zone with the host rocks (the Rudnoe and Kontaktovoe deposits) (Fig. 2). Because of this, the intrusion is now considered to be part of the regional Yenisei–Aldan metallogenic belt of marginal structures that surround the Siberian Platform [15] and extend from the southern margin of the Siberian Platform to Taimyr and include uniquely large PGE–Cu–Ni deposits in the Norilsk and Kodar–Udokan mining districts.

In contrast to most other layered ultrabasite–basite intrusions of the Baikal–Okhotsk belt, which also

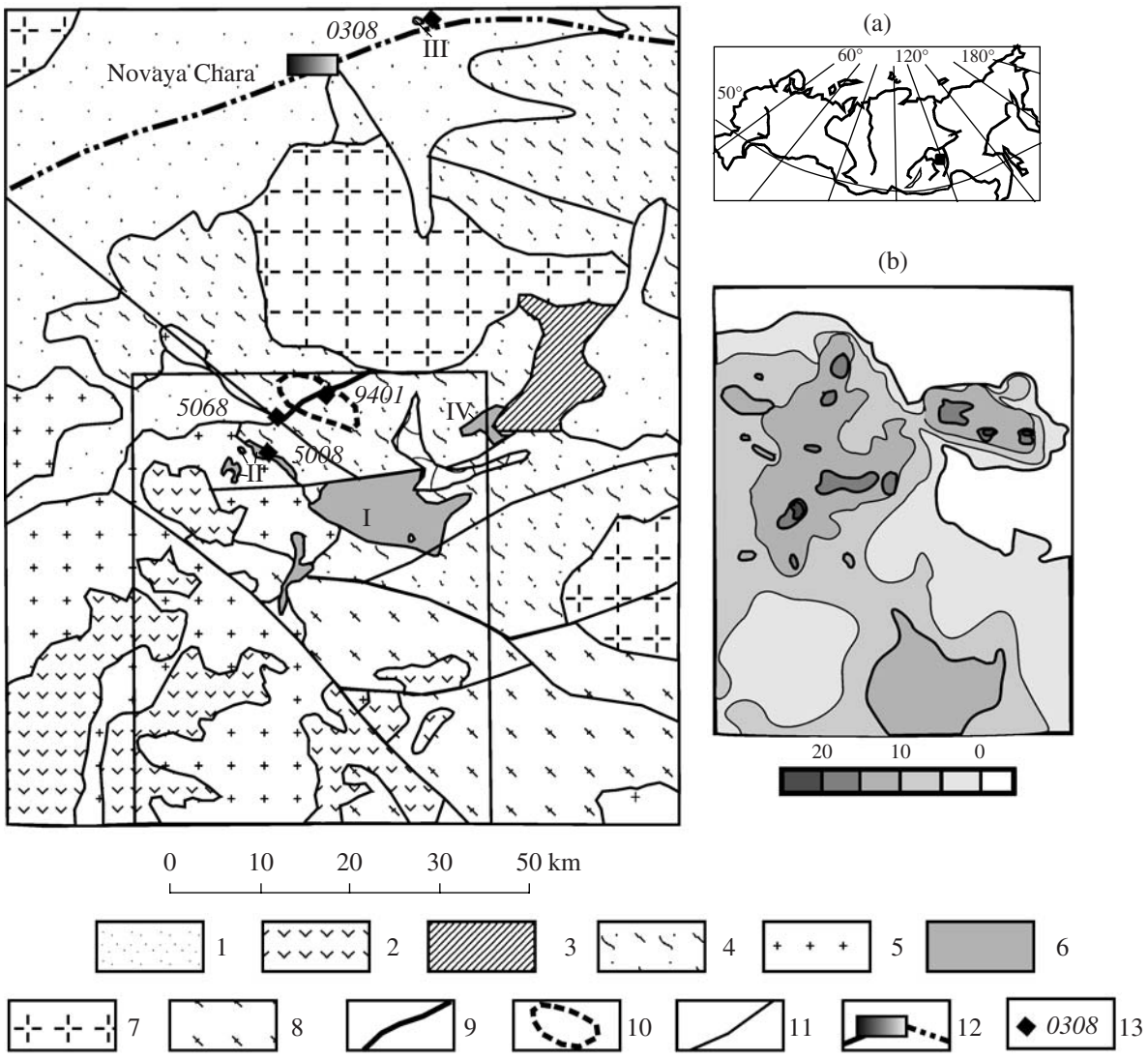

Fig. 1. Schematic geological map of the Kodar–Udokan district.

(1) Quaternary deposits; (2) Neogene–Quaternary volcanic rocks; (3) Vendian–Cambrian sedimentary deposits; (4) Early Proterozoic carbonate–terrigenous rocks of the Udokan Group; (5) granitoids of the Ingamakitskii Complex (Lukturskii Massif); (6) gabbroids of the Chineiskii Complex (massifs: I—Chineiskii, II—Mailavskii, III—Lukturskii, IV—Dorosskii); (7) granitoids of the Kodar Complex; (8) granitoids of the Kuandinskii Complex; (9) Main Dike of the Udokan deposit; (10) cupriferous sandstone bed at the Udokan deposit; (11) faults; (12) railway and station; (13) sampling sites and sample numbers. Insets: (a) Location map of the Kodar–Udokan district in Russia, (b) anomalous magnetic field in the area of the Chineiskii Massif (scale in μOe; modified after Sokol, 1978) as contour lines in a geological map.

includes the Chinneiskii Massif, the latter contains Fe richer basaltic rocks and widespread practically monomineralic petrographic varieties (clinopyroxenites, titanomagnetitites, and anorthosites) and is accompanied by deposits of oxide and sulfide ores. The complexity of the inner structure of the massif, the clearly pronounced layering and cyclicity of its rocks, and certain features of the related ore mineralization stimulated interest in this massif ever growing over several years [16–19 and others].

The massif is not, however, the only large magmatic body in the area in question. Its closest surrounding structures contain widespread irregularly shaped and tabular intrusions of basic rocks and numerous dikes, whose thickness occasionally reaches 200 m. Other large intrusions exposed north of the Chinneiskii Massif—the Lukturskii Massif—are associated with Cu–Ni ore mineralization. The separateness of the bodies and the scarcity of geochemical data on their rocks precluded the development of a comprehensive model for the evolution of magmatism in this part of the Kodar–Udokan trough.

Because of this, one of the tasks of our research was to study the spatial and genetic relations between the

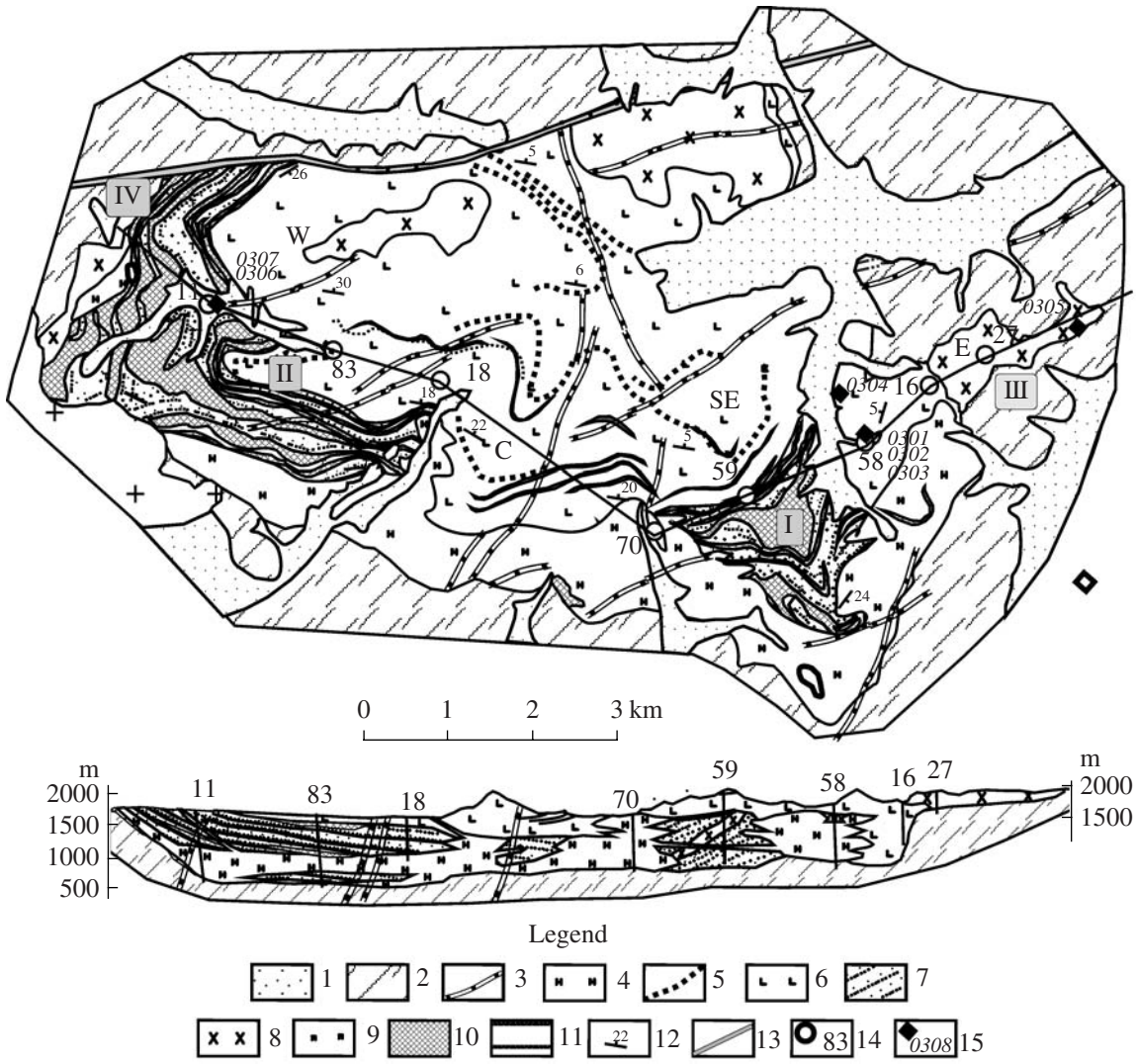

Fig. 2. Schematic geological map of the Chineiskii Massif.

(1) Quaternary deposits; (2) Early Proterozoic deposits of the Udokan Group; (*3*) basaltic dikes of various ages; (4–12) rocks of the Chineiskii Complex: (4) rocks of the gabbronorite series, (5) anorthosites, (6) rocks of the leucogabbro series, (7*)* rocks of the titanomagnetite–gabbro series, (8) monzodiorites, (9*)* pyroxenites (xenoliths), (10) high-grade titanomagnetite ores; (11) layers of titanomagnetite ore in the leucogabbro series; (12) strike and dip symbols of layering; (13) Ingamakitskii Fault; (14) boreholes and their numbers; (15) sampling sites and sample numbers. Ore deposits: (I) Magnitnoe, (II) Etyrko, (*III*) Rudnoe, (IV) Kontaktovoe. Blocks: *W*—western, *C*—central, *SE*—southeastern, *E*—eastern. The map was prepared with the use of materials of V.S. Chechetkin, V.K. Golev, V.K. Kryukov, N.V. Belova, E.G. Konikov, and others.

ultrabasite–basite intrusive bodies and their possible grouping within a single magmatic system, with the Chinneiskii Massif being its part. An important aspect of this study was the examination of the inner structure of the Chinneiskii Massif and the identification of the petrochemical features of its rocks as a clue to its genesis. Finally, our third task was to determine the phase characteristics of the parental magma of the massif and the composition of its melt and to evaluate the parameters of its crystallization.

These problems were solved based on the analysis of preexisting geological–geophysical data and the results of our geological and geochemical study of magmatic bodies in the Kodar–Udokan district. An important role was thereby played by detailed data on the inner structure of the Chinneiskii Massif, which were obtained in the course of its geological study. They allowed us to trace the relations between the main rock varieties and to characterize in much detail their layering. Numerous chemical analyses of the rocks were systematized with the application of cluster analysis, and the phase and chemical composition of the parental magma and its crystallization conditions were reproduced for each of the petrochemical types using the COMAGMAT-3.5 program. This publication presents these results.

FACTUAL MATERIALS

In studying the Chinneiskii Massif and its host rocks and structures, the authors used their original and available literature, geological, geophysical, and geochemical data. Satellite and aerial photographs were interpreted together with S.A. Abushkevich, and geophysical materials were interpreted together with A.F. Golovanov.

In the course of the fieldwork, traversing (60 km) with the documentation of primary exposures of basaltic rocks and their sampling was conducted concurrently with the detailed large-scale (1 : 10000) mapping of selected areas (30 km^2). Figures 1 and 2 show the sampling sites. Rocks from the layered series of the Chineiskii and Lukturskii massifs were studied in primary exposures (1500 m) and in the core of reference boreholes (holes 11, 83, 18, 70, 59, 58, 16, 27, and others; 4800 m).

The office processing of the materials involved the description of their petrographic thin sections (580 sections) and the analysis of their major rock-forming minerals on a JXA (GEOL) and a Cameca SX 50 microprobe at Moscow State University (analysts N.A. Krivolutskaya and N.N. Kononkova, 15 minerals). The analytical study also included XRF analyses of the rocks for major elements (at the Chita Institute of Natural Resources, Siberian Division, Russian Academy of Sciences, analysts N.S. Baluev, T.P. Mikhailova, L.M. Bad'ina, and V.P. Subbotina; and at Vernadsky Institute of Geochemistry and Analytical Chemistry, Russian Academy of Sciences, analysts I.A. Roshchina and T.V. Romashova; 117 analyses) and ICP-MS analyses for trace elements and REE (at the Institute of the Mineralogy, Geochemistry, and Crystal Chemistry of Rare Elements, analyst D.Z. Zhuravlev; and at the Institute of the Geology of Ore Deposits, Petrography, Mineralogy, and Geochemistry (IGEM), Russian Academy of Sciences, analyst S.A. Gorbacheva; 13 analyses).

GEOLOGICAL SETTING OF THE CHINEISKII MASSIF IN THE KODAR–UDOKAN ZONE

The Chineiskii Massif in northern Transbaikalia (Fig. 1, inset (a) is hosted in the Kodar–Udokan zone of the Siberian Platform. The zone has a complicated structure and underwent a long-lasting evolutionary history. A fragment of this zone is shown in Fig. 1. This area is characterized by a combination of meridional structures of the Chara–Olekma craton (Chara and Kalar blocks) and sublatitudinal Proterozoic structures of the Stanovoi mobile belt (Kadar–Udokan trough) [8, 20]. In the second half of the Paleoproterozoic, rifting in the northwestern Aldan–Stonovoi Shield [21] produced the large Udokan depression. A long-lived link of this crustal domain with the mantle follows from the occurrence of basic rocks of various ages in the Kalar and Udokan Ranges: these are Proterozoic gabbroids of the Chineiskii and Dorosskii complexes, Mesozoic volcanic–sedimentary deposits in the Chukchudinskii graben, and modern (dated at 2.1 ka) basaltic rocks in the Udokan lava plateau [22].

The magnetic and gravity fields of the Kodar–Udokan zone almost completely lie within a first-order structure: the Udokan regional gravity minimum, which is explained by the effect of thermal diapirs [23], which decreased the density of the crustal rocks and induced the development of a significant system of anticlinorium structures of the dome type [24]. The origin of these structures, which developed because of the remobilization of Archean rocks, is thought to have been related to multiphase magmatism in more permeable zones. These processes produced the Chineiskii basite complex.

Second-order features in the Udokan gravity minimum include two ring dome structures with similar inner structures of their gravity fields (Kemenskaya and Ingamakitskaya), which are characterized by a zonal structure. The marginal portions of these structures show elevated values of their gravity fields with local Δg and ΔT maxima above known (Chineiskii and Lukturskii) and inferred and unexposed basalt intrusions within fields of lower values. The geophysical data are in good agreement with the interpretations results, which suggest the occurrence of large ring structures, whose morphology and sizes correspond to the Imangakitskaya and Kemenskaya geophysical anomalies [25]. The Chineiskii pluton is restricted to the interference zone of these two ring structures.

In larger-scale (1 : 200000) maps of magnetic anomalies (Fig. 1, inset (b) and residual anomalous gravity field, the Chineiskii Massif is shown as the eastern termination of a field of high Δg and ΔT values. The central part of this field is much greater than the part of the Chineiskii Massif exposed at the surface. The anomalous values of these geophysical parameters are caused by gabbroid exposures among granitoids of the Ingamakitskii Complex of Late Paleozoic age or, within the Upper Chara depression, by the Lukturskii Massif, which is partly overlain by Neogene–Quaternary sedimentary rocks (Fig. 1). The Main Gabbronorite Dike of the Udokan deposit, which lies on the northward continuation of the axes of the anomalies, is also classed with the Chineiskki Complex [26].

The facts presented above lead to the conclusion that, with regard for geophysical data, the actual field of the rocks of the Chineiskii Complex is larger than that outlined based on their separate exposures. For example, we believe that the Chineiskii intrusion is merely a fragment of a large magmatic system discovered in this area, and the intrusion is made up of a number of rock groups, whose relations and genesis remain largely disputable, in spite of fact that these rocks were studied for a long time: from 1938 until 2006.

The genesis of the Chineiskii Massif is reportedly related to the termination of collision processes in the Olekma granite–greenstone belt [27]. This conclusion

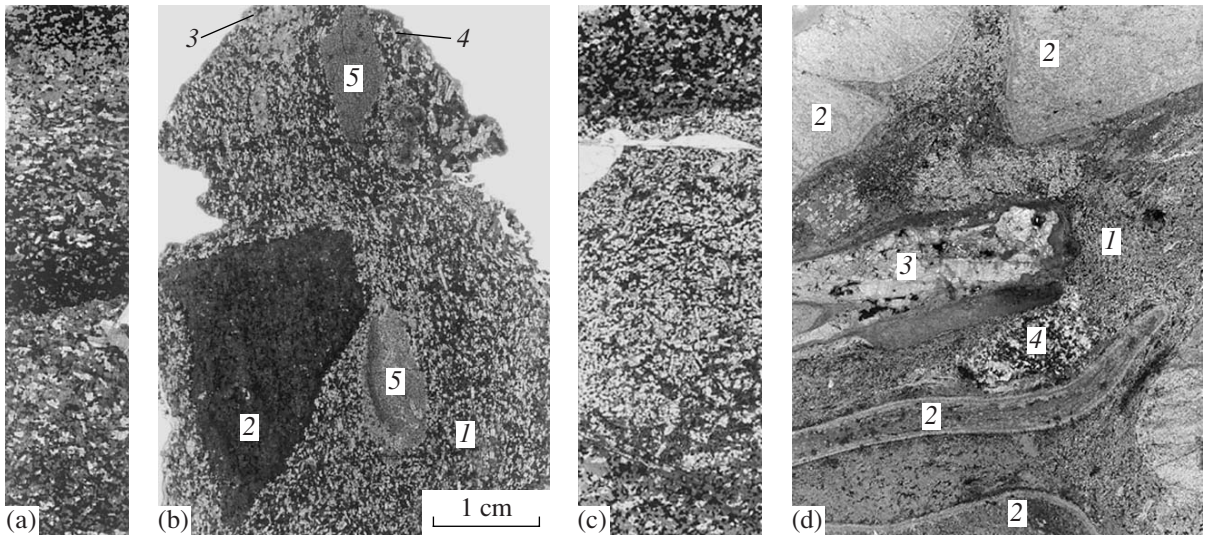

Fig. 3. Micrographs of rocks (in thin sections) from the Chineiskii Massif (2/3 downscaled). (a) Contact of two microrhythms in rocks of the titanomagnetite series (here and in Figs. 3b–d, black is titanomagnetite, gray is pyroxenes, and white is plagioclase); (b) magmatic breccias with (*1*) titanomagnetite-gabbronorite cement and fragments (*2*—pyroxenites, *3*—anorthosites, *4*—monzodiorites, *5*—sandstones); (c) leucocratic segregation in gabbroid of the gabbronorite series; (d) magmatic breccias with (*1*) lamprophyre cement and fragments (*2*—metamorphosed sandstones, *3*—skarns, *4*—gabbroids).

is based on the zircon dates of the Kemenskii granitoid massif (1873.1 ± 2.5 Ma), which is cut by the gabbroids of the Chineiskii Complex, and the K–Ar amphibole age of the Chineiskii Massif (1830 + 50 Ma [28]).

INNER STRUCTURE OF THE CHINEISKII MASSIF

Overview. The intrusion is an asymmetrical lopolith-shaped body, whose floor dips at angles of 10–25° centerward in the western part of the body and lies nearly horizontally near the surface (at depths of a few dozen meters) in its eastern part. The northern contact of the intrusion is tectonic (Fig. 2). The total thickness of the massif (with regard for its upper part exposed at the surface and the lower part penetrated by boreholes) is 2.5 km. It is hosted by Lower Proterozoic rocks of the Udokan Complex and is cut by the Paleozoic granites of the Imangakit Complex in the southwest [29, 17].

The massif is characterized by a complicated inner structure. In contrast to classic layered plutons, whose layers can be traced for dozens and even hundreds of kilometers [5, 30], the Chineiskii intrusion shows no such well-pronounced layering throughout its whole volume. The massif consists of notably different four blocks: western, central, eastern, and southeastern. For example, the western and southeastern blocks are characterized by the presence of clearly layered rocks with elevated titanomagnetite contents in the gabbroids, while the central and eastern blocks are dominated by massive rock varieties. The southeastern part of the intrusion contains much xenoliths of the host carbonate rocks, which make the inner structure of the massif much more complicated, because the gabbroids are strongly contaminated by rocks of the Udokan Formation.

The massif is composed of a number of rock groups with intrusive relations between them [31, 32]:

(I) The first group comprises large xenogenic blocks and xenoliths of pyroxenites (up to 80 m across), altered anorthosites, and gabbro (Fig. 2). They are surrounded by chill zones of the host gabbroids: these are fine-grained gabbro and gabbronorite zones ranging from a few centimeters to a few decimeters in thickness. Clinopyroxenites were also found in the central parts of the massif but are spread much more widely in its peripheral portions, particularly in the eastern termination of the intrusion. They were found in the form of angular fragments in the magmatic breccias (Fig. 3b) and consist of clinopyroxene (augite and diopside-augite), which is accompanied (in coarser grained and pegmatoid varieties) by olivine ($Fa_{55–59}$, up to 5–10%, Table 1), biotite, and plagioclase. "Altered anorthosites" [29] were found as podiform bodies and rounder or equant xenoliths (up to 20 m long) and are strongly altered, with their plagioclase replaced by prehnite and mafic minerals, such as micas, amphiboles, magnetite, and sphene.

(II) The second rock group includes gabbroids with elevated contents of titanomagnetite, which are classified into a titanomagnetite gabbro (approximately 1.0 km thick) and a leucogabbro (up to 1.5 km) series. The rocks of the titanomagnetite gabbro series occur as two separated blocks (western and southeastern, Fig. 2). The leucogabbro series (massive gabbro, leucogabbro, and anorthosites with layers of massive titanomagnetite ores) are exposed at the surface in the central block and

Table 1. Composition of olivine and pyroxenes in rocks from (1–13) the Chineiskii and (14–15) Lukturskii massifs

Component	1	2	3	Component	4	5	6	7	8	9	10	11	12	13	14	15
	sample				sample											
	0302a	0302b	0302c		0301	0306	0307a	0307b	0307c	0304a	0304b	0304c	0303a	0303b	0308a	0308a
SiO_2	33.35	33.99	33.94	SiO_2	53.11	52.00	53.92	53.74	53.76	51.75	52.00	52.11	52.86	51.70	51.49	51.72
TiO_2	0.01	0.00	0.00	TiO_2	0.00	0.57	0.24	0.32	0.29	0.22	0.17	0.35	0.29	0.45	0.30	0.26
Al_2O_3	0.00	0.00	0.02	Al_2O_3	0.08	2.12	1.36	1.21	1.11	1.03	0.58	1.08	1.29	1.95	0.50	0.45
Cr_2O_5	0.00	0.01	0.01	Cr_2O_5	0.03	0.02	0.00	0.00	0.00	0.01	0.00	0.02	0.00	0.01	0.07	0.04
FeO	46.46	48.37	45.56	FeO	11.21	9.37	18.75	19.01	19.01	12.00	28.10	12.14	23.16	12.04	29.85	29.92
MgO	19.42	19.42	20.26	MgO	12.05	14.95	23.62	24.74	25.33	13.15	18.85	13.33	21.96	14.69	17.01	17.32
CaO	0.09	0.03	0.07	CaO	23.39	20.86	2.99	1.46	1.18	20.64	0.89	20.18	1.67	18.78	1.71	1.10
				Na_2O	0.08	0.29	0.01	0.05	0.00	0.25	0.03	0.27	0.00	0.31	0.00	0.00
				K_2O	0.01	0.00	0.01	0.00	0.00	0.01	0.02	0.00	0.00	0.01	0.01	0.00
Total	99.33	101.82	99.86	Total	99.95	100.17	100.91	100.53	100.67	99.06	100.63	99.48	101.24	99.92	100.94	100.81
Fo	42.45	41.72	43.97	*Wo*	47.57	42.06	5.90	2.87	2.29	42.35	1.80	41.34	3.31	38.09	3.48	2.26
Fa	56.96	58.28	55.46	*En*	34.11	41.95	64.83	67.50	68.51	37.54	53.10	38.01	60.47	41.47	48.33	49.33
Tp	0.58	0.00	0.57	*Fs*	18.03	14.93	29.23	29.47	29.20	19.17	44.98	19.66	36.22	19.31	48.19	48.41
				Ac	0.29	1.05	0.04	0.16	0.00	0.94	0.12	0.99	0.00	1.13	0.00	0.00

Note: (1–3) Olivine and (4–5) pyroxenes form rocks of the Chineiskii Complex. (4) Clinopyroxenites of group I; (5–8) titanomagnetite-bearing gabbro and (9–11) gabbronorites of group 2; (12–13) norites of group 3; (14–15) norites from the Lukturskii Massif.

compose the upper part of the massif, whose apical part includes exposures of gabbrodiorites and monzodiorites with numerous xenoliths of the host rocks.

(III) The third rock group comprises norites and gabbronorites, which are recognized as the norite series and whose rocks are exposed in the central block and occur near the bottom of the western and southwestern blocks. The thickness of the series increases from 300 to 800 m from west to east. The norites and gabbronorites often penetrate the overlying rocks of the second group (titanomagnetite gabbro) in the form of sills and tongues. Their chill zones are pronounced very poorly (are no thicker than a few centimeters) or are absent (perhaps, because the temperatures of the newly emplaced melt and the still hot, but already crystalline, magmatic rocks were similar). The southern part of the massif displays remarkable angular unconformities between layering in the norite series and the titanomagnetite gabbro and leucogabbro series. This fact provides additional evidence that the emplacement of the main rock groups was separated by a certain time span.

(IV) The youngest rocks are magmatic breccias with a lamprophyre and gabbronorite cement (Figs. 3b, 3d) and lamprophyres, which compose sills (a few meters thick) near the bottom of the intrusion, dikes, and chimneys (a few meters in diameter) in the massif.

The fractions of various rocks in the massif vary: the massif is dominated (~90%) by the rocks of the second and third groups (in the proportion of approximately 2 : 1), whereas xenoliths and magmatic breccias account for only 5% of the total intrusion volume each. The strikes and dips of the two major rock groups are usually similar: they dip toward the center of the massif at angels varying from 3° to 10–15° in the central part and 40–45° in the western part, at contacts with granitoids of the Ingamakitskii Complex. The dips of the rocks of the titanomagnetite–gabbro series in the southern part of the massif are opposite (southward at angles of 25–30°), a fact previously explained [32] by the unevenness of the massif bottom. The aforementioned inconsistencies between the dips and strikes of rocks of the titanomagnetite gabbro series and the surrounding norites in this area and the seemingly intrusive relations between them suggest that a large block of the second-group gabbroids occur among the younger gabbronorites.

The major rock groups (second and third) exhibit clearly pronounced and variable layering. Its first type can be characterized as low-scale (from a few centimeters to a few decimeters) layering due to variations in the contents of mafic minerals in the vertical sections of certain rock layers, which are usually closely similar in bulk composition (so-called gravitational stratification, [2], (Fig. 3a) which is manifested in alternating compositionally contrasting and relatively thick, up to a few meters, layers of anorthosites, massive gabbro, gabbronorites, and titanomagnetitites). This type of layering is particularly characteristic of the upper part of the massif (leucogabbro series).

The rocks of the Chineiskii Massif were also determined to display rhythmicity at various scales due to systematic rock variations in rhythmic units (from bottom to top) from melanocratic to leucocratic varieties, as is typical of many layered plutons worldwide (for example, Bushveld and Skaergaard). The layered units recognized in the massif include not only the aforementioned series (titanomagnetite gabbro, leucogabbro,

and norite up to 1.5 km thick) but also smaller scale units, such as rock units (a few hundred meters), rhythms (a few dozen meters), and, finally, microrhythms (from a few centimeters to a few decimeters).

Structure of the vertical section of the massif. Figure 4 shows a generalized vertical section of the Chineiskii Massif, which characterizes the western block of the pluton. Its lower part was examined using materials from Hole 83, and its upper part (up to the apical zone of the intrusion) was studied in primary exposures. The section shows all of the aforementioned major rock groups composing the massif: norites, gabbronorites, and anorthosites, with both accessory titanomagnetite and its elevated concentrations (10–80 vol %), up to massive titanomagnetite ores. From its bottom to top, the vertical section of the massif consists of a number of zones that differ in composition and inner structure.

For instance, the lower zone (200 m thick) consists of gabbroids and anorthosites with titanomagnetite. Its cumulus minerals are titanomagnetite (Ti-*Mt*) and plagioclase (*Pl*). The rhythmic layering of this zone is pronounced weakly. The zone is dominated by coarse-grained gabbro, leucogabbro, and anorthosites, which consist mostly of plagioclase ($An_{50–55}$) and titanomagnetite with minor admixtures of orthopyroxene. Titanomagnetite typically occurs as euhedral grains among large tabular unzoned plagioclase crystals (Figs. 3–5).

This zone is overlain by a zone dominated by norites with subordinate amounts of gabbronorites and leucogabbro (norite series approximately 400 m thick). The composition of the cumulus minerals (orthopyroxene ± plagioclase) varies within $En_{59–61}$ $Fs_{36–38}$ Wo_3 (Table 1) and $An_{50–60}$ (Figs. 5, 6). The rhythmic layering of the rocks is pronounced clearly enough and is accentuated by variations in the chemical composition of the rocks, because compositionally uncontrasting rocks systematically alternate in rhythmic units in the vertical section: the pyroxenites grade into norites and then gabbronorites. The thicknesses of the individual units are thereby 1.5–2 m.

The central part of the vertical section consists of the rocks of the titanomagnetite–gabbro series (700 m thick), which are characterized by clearly pronounced layering. The cumulus mineral is clinopyroxene $En_{37–42}$ $Fs_{15–20}$ $Wo_{38–42}$ (or clinopyroxene + titanomagnetite) in the lower parts of the rhythmic units and plagioclase of the composition $An_{52–57}$ in their upper parts. The rocks are dominated by clinopyroxene (Fig. 5-5), although many rock units contain, along with this mineral, also orthopyroxene $En_{53–68}$ $Fs_{29–45}$ $Wo_{2–3}$ and inverted pigeonite. The rocks of the titanomagnetite gabbro series often have trachytoid structures (Fig. 5-4) and sometimes contain xenoliths of the first-group pyroxenites (Fig. 4).

Farther up the vertical section, these rocks give way to the leucogabbro series (800 m), which consists of predominant anorthosites (Fig. 5-1) and leucogabbro. These rocks are enriched in titanomagnetite in the lower part (these varieties are referred to as *chinites*, Fig. 5-2 [34]) with beds of massive titanomagnetite ores. The main cumulus minerals are $An_{47–57}$ and, in rocks rich in titanomagnetite, also titanomagnetite (Ti-*Mt* ± *Pl*). The rocks contain subordinate concentrations (no more than 10 vol %) of clinopyroxene $En_{37–38}$ $Fs_{19–20}$ $Wo_{40–42}$. The apical part of the massif is made up of monzodiorites and quartz diorites, which often have a granophyric texture.

The composition of cumulus in discrete zones in the vertical section varies unsystematically: *An* + Ti-*Mt* – *Opx* ± *Pl* – *Cpx* ± *Mt* – *An* ± Ti-*Mt*.

The contrasting structure of this section is accentuated by the distribution of major oxides, first of all, MgO and TiO_2 (Fig. 4). The rocks of the norite series are characterized by an elevated content of MgO (9.3 wt % on average, as compared to 5.7 wt % in the titanomagnetite gabbro series), and the low contents of oxide minerals cause relatively low concentrations of Fe and Ti (1.1 wt % against 2.6 wt % in the titanomagnetite gabbro series). While the titanomagnetite gabbro series displays pervasively high TiO_2 concentrations, the rocks of the same group in the leucogabbro series exhibit a saw-shaped TiO_2 distribution due to alternating anorthosites and gabbroids enriched in titanomagnetite (Table 2, Figs. 4, 7).

As was mentioned above, the recognized series consist of variable numbers of rock units. For example, the titanomagnetite gabbro series consists of five units, while the norite one comprises only three. This is clearly manifested in the ratio of "magnetite" iron to the total iron concentration in the rocks FeO_{Mt}/FeO_t, with the latter determined separately by conventional chemical techniques at the Central Laboratory of the Chitageologia, and in the variations of TiO_2 and V_2O_5, which are more typical of the titanomagnetite gabbro series (Fig. 6). The same series is characterized by clearly pronounced layering, which could be caused by the gravitational accumulation of titanomagnetite near the bottom of layers. Boundaries between microrthythms are usually sharp and clear (Table 3, Fig. 7). In the direction from the lower to upper contact, interstitial anhedral plagioclase appears, with the size of its grains gradually increasing in the same direction. These grains compose lenses and then layers, in which plagioclase acquires a euhedral habit [35, 32]. Rare sulfides are usually restricted to leucocratic segregations in the upper parts of the rhythms, although they were also often found in the lower parts of the rhythms. The data presented above (Figs. 6, 7) show that the titanomagnetite gabbro series is characterized by clearly pronounced rhythmicity of variable scale: microrthythms, rhythms, and units with a systematic gradation of titanomagnetite gabbro into anorthosites enriched in titanomagnetite (chinites).

Table 2. Composition of rocks from the vertical section of the massif

No.	SiO_2	TiO_2	Al_2O_3	Fe_2O_3	MnO	MgO	CaO	Na_2O	K_2O	P_2O_5	LOI	Total	Sample
1	53.79	2.40	13.94	14.75	0.23	1.63	6.56	3.83	1.70	0.70	0.47	100.00	321/1
2	53.77	2.12	15.93	11.76	0.24	1.45	5.67	4.85	2.95	0.54	0.71	100.00	321/2
3	56.82	1.82	15.94	11.35	0.20	1.63	6.15	3.40	1.66	0.60	0.43	100.00	321/4
4	42.44	2.93	11.37	21.68	0.22	6.63	10.74	2.38	0.62	0.10	1.16	100.27	522
5	43.61	2.49	13.07	20.10	0.18	5.79	10.20	2.79	0.92	0.09	0.06	99.30	521
6	44.98	2.48	13.62	19.87	0.18	5.80	11.00	2.96	0.67	0.11	0.18	101.82	520
7	43.09	2.69	12.42	20.05	0.21	6.91	12.11	2.88	0.42	0.07	0.00	100.85	519
8	42.94	2.68	13.21	19.23	0.2	6.68	11.52	2.87	0.39	0.11	0.38	100.21	518
9	45.58	2.29	13.87	17.84	0.19	6.44	11.96	2.79	0.47	0.07	0.34	101.85	517
10	44.83	2.31	12.85	17.70	0.19	6.52	12.21	2.64	0.52	0.06	0.14	99.97	516
11	39.77	3.34	9.88	23.49	0.22	7.77	11.93	2.28	0.35	0.08	0.29	99.38	515
12	51.42	0.61	13.91	9.99	0.21	11.42	8.93	2.40	0.35	0.06	0.44	99.73	514
13	47.97	1.59	23.69	9.77	0.06	1.27	10.34	4.07	0.73	0.08	1.35	100.93	513
14	43.40	2.15	18.87	17.30	0.11	3.03	9.67	4.35	0.68	0.09	0.20	99.85	512
15	46.16	1.64	14.54	15.88	0.16	6.16	12.26	3.71	0.39	0.07	0.38	101.34	511
16	52.61	0.31	24.14	4.93	0.05	1.10	9.90	4.14	1.25	0.28	1.62	100.34	510
17	46.15	2.17	14.86	16.16	0.02	5.65	12.2	2.96	0.44	0.07	0.16	100.83	509
18	47.98	1.66	12.06	15.85	0.21	7.47	12.08	3.39	0.60	0.12	0	101.40	508
19	46.11	1.89	14.26	15.35	0.16	6.07	11.31	3.03	0.62	0.10	0.20	99.10	507
20	48.67	1.49	14.05	14.15	0.2	7.12	11.41	3.00	0.49	0.07	0.17	100.81	506
21	45.77	2.02	21.58	13.69	0.07	1.28	9.00	4.13	1.00	0.09	1.32	100.65	505
22	46.82	1.79	14.94	15.97	0.18	6.13	10.79	3.93	0.61	0.08	0.18	101.43	504
23	38.09	3.77	8.07	26.59	0.29	9.28	11.74	2.46	0.28	0.05	–0.47	100.14	503
24	43.45	2.43	13.76	18.46	0.20	6.17	11.34	3.42	0.53	0.11	0	99.85	502
25	45.98	2.01	14.10	16.29	0.19	6.3	11.38	2.89	0.51	0.08	0.11	99.82	501
26	49.55	0.78	22.50	8.55	0.08	2.47	10.51	3.22	0.61	0.14	1.11	99.51	8300201
27	46.54	1.43	16.20	15.97	0.16	7.65	8.04	2.49	0.53	0.09	0.51	99.61	8300388
28	43.03	2.82	18.83	19.35	0.13	3.00	8.89	3.05	0.49	0.08	–0.13	99.54	8300600
29	33.36	4.69	16.49	32.19	0.12	1.70	7.47	3.68	0.39	0.03	0.52	100.64	8300800
30	32.32	4.62	17.91	32.95	0.12	1.87	6.44	3.16	0.46	0.02	0.30	100.16	8301400
31	23.34	7.19	14.34	45.65	0.16	2.07	5.45	2.98	0.33	0.02	–0.34	101.20	8301600
32	42.96	2.76	15.91	19.91	0.14	4.48	10.82	2.64	0.39	0.03	–0.09	99.95	8301786
33	45.28	2.17	11.96	19.81	0.19	6.68	12.10	2.25	0.49	0.03	0.29	101.24	8302000
34	44.93	1.96	13.86	17.69	0.17	5.98	11.26	2.58	1.09	0.02	1.85	101.38	8302200
35	43.31	2.80	16.56	22.04	0.15	4.80	8.23	2.74	0.53	0.03	0.23	101.41	8302400
36	52.03	0.64	17.21	10.36	0.16	5.76	9.88	2.83	0.65	0.04	0.68	100.23	8302600
37	51.68	0.64	17.05	11.49	0.14	6.14	8.96	2.69	0.73	0.06	1.11	100.69	8302830
38	45.94	1.36	16.38	15.90	0.14	4.38	10.10	4.75	0.69	0.08	1.55	101.25	8303000
39	45.85	1.83	13.92	17.28	0.16	6.91	10.14	2.48	0.49	0.03	2.80	101.87	8303202
40	43.12	2.92	13.27	20.22	0.18	6.46	10.33	2.24	0.52	0.03	1.15	100.44	8303366
41	44.65	1.84	12.36	17.16	0.17	7.96	11.75	2.37	0.49	0.03	0.37	99.15	8303655
42	46.16	1.69	15.08	16.47	0.17	6.12	12.02	2.79	0.61	0.02	0.31	101.44	8303805
43	45.00	1.77	13.11	18.88	0.20	7.41	11.34	2.43	0.32	0.02	–0.31	100.16	8304000
44	46.46	1.91	13.70	16.85	0.18	6.42	12.07	2.27	0.40	0.03	0.71	100.99	8304200
45	49.83	0.87	15.11	12.06	0.14	6.52	13.15	2.18	0.32	0.02	0.42	100.62	8304401
46	40.26	2.73	11.87	24.15	0.19	6.92	10.87	2.41	0.34	0.03	0.25	100.01	8304602
47	44.63	2.26	15.42	18.51	0.17	5.76	10.83	2.71	0.48	0.03	0.33	101.12	8304800
48	35.68	4.29	13.21	32.34	0.16	4.42	6.61	3.21	0.43	0.02	0.51	100.88	8305202

Table 2. (Contd.)

No.	SiO_2	TiO_2	Al_2O_3	Fe_2O_3	MnO	MgO	CaO	Na_2O	K_2O	P_2O_5	LOI	Total	Sample
49	43.44	2.77	13.18	22.28	0.20	6.30	10.95	2.33	0.42	0.04	–0.36	101.56	8305400
50	37.99	3.49	14.30	26.55	0.16	4.57	9.51	2.93	0.45	0.03	–0.39	99.57	8305600
51	45.25	3.01	13.82	19.99	0.19	5.69	7.90	2.53	0.45	0.03	0.43	99.29	8305617
52	44.23	3.03	12.90	20.69	0.20	6.30	10.31	2.32	0.48	0.03	–0.08	100.40	8305800
53	34.07	4.20	14.35	31.88	0.16	4.21	8.59	2.42	0.38	0.02	0	100.27	8306000
54	37.71	3.63	14.08	27.67	0.16	3.74	9.35	3.50	0.66	0.04	0.28	100.82	8306200
55	34.32	4.54	12.37	32.12	0.14	4.77	8.28	3.31	0.34	0.02	0.84	101.06	8306400
56	47.79	1.50	15.20	15.35	0.17	5.85	12.14	2.97	0.59	0.06	0	101.62	8306600
57	43.64	2.50	13.60	20.75	0.19	6.18	10.06	2.78	0.68	0.09	0.22	100.69	8306803
58	45.33	1.60	13.27	19.22	0.22	7.89	10.74	2.50	0.39	0.03	0.42	101.60	8307000
59	44.97	1.68	14.96	15.46	0.16	5.85	9.55	2.62	0.87	0.07	4.43	100.62	8307197
60	40.29	3.29	12.28	24.38	0.21	6.78	10.25	2.65	0.45	0.05	–0.46	100.17	8307380
61	40.44	2.70	14.86	23.77	0.15	4.08	9.57	2.48	0.48	0.04	–0.23	99.07	8307600
62	35.00	5.48	16.97	27.81	0.14	1.77	7.63	3.36	0.56	0.03	0.31	99.06	8307815
63	45.95	1.97	12.37	18.39	0.19	6.92	9.71	2.39	1.05	0.07	0.37	99.37	8308000
64	44.62	2.23	13.58	20.43	0.20	7.89	7.39	2.50	0.54	0.04	0.23	99.65	8308200
65	48.93	1.22	14.97	14.56	0.20	8.43	7.68	2.66	0.81	0.08	0	99.54	8308400
66	50.99	0.78	15.14	12.61	0.19	8.26	7.26	2.58	0.78	0.07	0.61	99.26	8308628
67	50.57	0.91	18.96	10.45	0.13	5.33	8.95	2.58	1.02	0.10	1.96	100.94	8308875
68	51.25	0.90	15.54	12.46	0.17	7.68	8.08	2.28	1.06	0.09	1.84	101.34	8309032
69	49.04	1.33	13.98	15.92	0.19	9.32	6.97	2.21	0.99	0.09	1.34	101.37	8309270
70	47.41	1.76	9.20	21.69	0.27	12.4	5.67	1.79	0.71	0.08	0.07	101.05	8309286
71	48.29	1.42	12.28	18.80	0.20	9.18	6.37	2.56	0.77	0.06	–0.1	99.83	8309406
72	49.21	0.93	12.45	16.04	0.20	10.59	6.84	2.87	0.92	0.09	0.68	100.82	8309610
73	49.13	0.91	15.47	13.16	0.16	7.64	8.15	2.44	0.95	0.08	0.95	99.04	8309812
74	49.72	1.20	11.61	16.73	0.23	10.41	6.88	3.64	0.92	0.09	0.29	101.70	8310000
75	42.45	2.10	9.93	26.72	0.23	10.93	5.48	2.39	0.57	0.06	–0.61	100.25	8310208
76	49.94	1.22	10.88	16.55	0.22	11.18	6.67	2.73	0.85	0.07	0.43	100.73	8310365
77	46.58	0.87	12.92	17.55	0.18	8.96	7.12	2.30	0.73	0.06	1.85	99.11	8310410
78	56.26	1.01	19.02	9.62	0.07	3.46	1.21	3.45	4.28	0.11	0.82	99.29	8310620
79	50.63	1.36	11.73	16.64	0.21	9.19	7.55	3.68	0.86	0.08	0	101.92	8310800
80	53.51	1.28	18.24	8.44	0.18	7.23	9.18	2.48	0.82	0.03	0.29	101.67	8311012
81	51.03	1.16	12.37	13.60	0.23	12.17	6.80	1.80	0.66	0.04	–0.17	99.69	8311226
82	46.88	2.13	14.31	18.76	0.16	4.75	9.50	2.42	0.91	0.09	0	99.91	8311435
83	41.29	3.17	12.18	26.56	0.24	6.38	5.95	2.35	1.41	0.12	0.36	100.02	8311600
84	50.18	0.67	9.07	10.09	0.16	10.91	17.88	1.76	0.37	0.07	0.65	101.79	8311800
85	40.67	3.94	16.83	25.36	0.16	3.34	7.83	2.91	0.99	0.09	–0.4	101.73	8312004
86	46.65	2.44	14.79	18.19	0.17	4.94	9.14	3.18	1.15	0.12	0.34	101.10	8312200
87	43.52	2.67	15.44	21.89	0.14	4.16	8.03	2.57	0.98	0.09	0	99.49	8312400
88	37.80	3.66	13.99	28.33	0.15	4.26	6.85	3.29	1.68	0.08	0.34	100.44	8312610
89	51.44	1.24	13.94	14.59	0.17	6.66	7.62	2.24	1.24	0.090	1.03	100.26	1112750
90	53.81	0.81	18.10	9.76	0.12	4.42	8.58	2.45	0.95	0.120	0.94	100.06	1112845

Note: (1) Analyses were made by XRF (analysts N.S. Baluev, L.M. Bad'ina, T.P. Mikhailova; Chita Institute of Natural Resources, Siberian Division, Russian Academy of Sciences); (2) analysis numbers correspond to the following series: 321/1–321/3, and 501–522—leucogabbro; 8300201–8308875—titanomagnetite gabbro; 8309032—gabbronorite; 1112750–1112845—lamprophyres, Hole 11; (3) samples for the analyses were taken at sites spaced 20 m apart in Hole 83 and above it (from exposures). Seven-digit numbers: the first two digits correspond to the hole number, and the third through seventh digits correspond to the depths (in decimeters).

Table 3. Rock compositions (wt %) in microrhythms

Depth, cm	Rhythm no.	SiO_2	TiO_2	Al_2O_3	Fe_2O_3	FeO	MnO	MgO	CaO	Na_2O	K_2O	P_2O_5
68	5	17.82	8.84	4.07	27.26	29.51	0.29	6.73	3.47	1.79	0.20	0.01
69		18.67	8.74	3.61	28.41	28.06	0.31	6.58	3.94	1.48	0.19	0.01
71	4	41.42	3.36	7.21	10.12	16.89	0.26	9.96	9.35	0.98	0.37	0.08
73		35.49	4.67	6.81	15.11	19.84	0.28	8.81	7.76	0.94	0.26	0.03
74		30.81	5.74	6.03	19.41	21.95	0.30	9.12	5.30	1.01	0.30	0.03
75		21.41	8.13	4.33	26.47	27.77	0.32	7.05	3.27	0.99	0.24	0.03
76		17.02	9.05	3.40	29.92	29.62	0.31	6.91	2.14	1.43	0.19	0.01
78	3	33.84	5.09	5.42	16.84	22.66	0.32	10.40	4.17	0.92	0.29	0.05
79		28.45	6.70	5.71	21.06	23.73	0.31	9.15	3.68	0.94	0.25	0.02
80		23.64	7.53	4.77	26.79	25.23	0.32	7.31	3.21	0.95	0.23	0.02
81		19.99	8.50	4.43	27.49	27.93	0.30	7.43	2.86	0.86	0.21	0.01
83	2	49.92	1.58	18.48	1.07	12.74	0.13	4.15	9.02	2.36	0.49	0.06
84		45.26	2.51	8.53	7.85	17.08	0.28	10.88	5.88	1.27	0.42	0.04
85		43.34	2.91	7.75	10.33	17.25	0.29	10.97	5.68	1.09	0.33	0.06
86		37.08	4.45	5.37	13.79	21.94	0.32	11.63	4.14	0.99	0.24	0.05
87		30.25	6.13	4.11	19.15	24.77	0.32	10.49	3.59	0.98	0.20	0.02
89	1	48.17	1.94	14.20	8.32	9.57	0.19	6.51	8.42	2.12	0.48	0.08

Note: Analyses were made by XRF (analysts N.S. Baluev, L.M. Bad'ina, T.P. Mikhailova; Chita Institute of Natural Resources, Siberian Branch, Russian Academy of Sciences); samples were taken from the core of Hole 11, depth interval 622.68–622.89 m.

Classification of Rocks According to Their Petrochemistry

The data presented above on the Chineiskii Massif testify that its inner structure is notably heterogeneous, as is pronounced in the variations in the chemical and mineralogical composition of the rocks, often on a small scale (from a few meters to a few centimeters, Figs. 4, 6, 7). All available chemical analyses (847 analyses) did not allow us to clearly distinguish between some rock varieties composing the intrusion. The closest similarities were shown by the two major rock groups dominating in the massif: the titanomagnetite gabbro and leucogabbro series of the second group and the norite series of the third group. Clearly distinct rocks are only those of the second group (pyroxenites because of their elevated MgO concentrations) and the fourth group (magmatic breccias with a lamprophyre cement) because of their elevated concentrations of SiO_2 and alkalis (Table 2).

At the same time, the analysis of geological and petrochemical data led us to suggest that relatively pervasively occurring types (rock varieties) exist, and their compositions were controlled by the evolution of the parental magma and may now systematically alternate in the vertical section of the massif. In order to reveal them and their possible pervasively occurring relations in the vertical section, we conducted the petrochemical systematization of the magmatic rocks using a technique developed at the Department of Geochemistry of Moscow State University approximately three decades ago and then applied to describe the inner structures of the Kivakka [36] and Ioko-Dovyren [37] layered intrusions. This approach makes it possible to optimize the processing of large massifs of heterogeneous petrochemical data: to identify representative compositions that can then be used to evaluate the composition of the parental magma and the conditions under which it crystallized.

The method of petrochemical systematization of rocks relies on the utilization of a computer program with the hierarchical clustering of objects according to formal criteria by the Ward algorithm [38]. In application to a set of chemical characteristics, this principle involves the successive grouping of the compositions with the minimum increment of the average "geochemical state" of the compositions combined into groups at each step [37]. This approach involves calculation in Euclidian metrics with the use of the relative concentrations normalized to the dispersion for each component in the initial selection of the compositions. This procedure makes it possible to bring the concentrations of various components to a single scale and thus to make their contributions to the calculation of the "compactness" of the clusters comparable. Rocks of the Chineiskii Massif were classified by this method using a version of the PETROTYPE clustering computer program, which was designed and developed at the Vernadsky Institute of Geochemistry and Analytical Chemistry, Russian Academy of Sciences, for the purposes of the petrochemical systematics of volcanic and subvolcanic rocks [39]. In order to identify persistently occurring petrochemical rock types, we used the con-

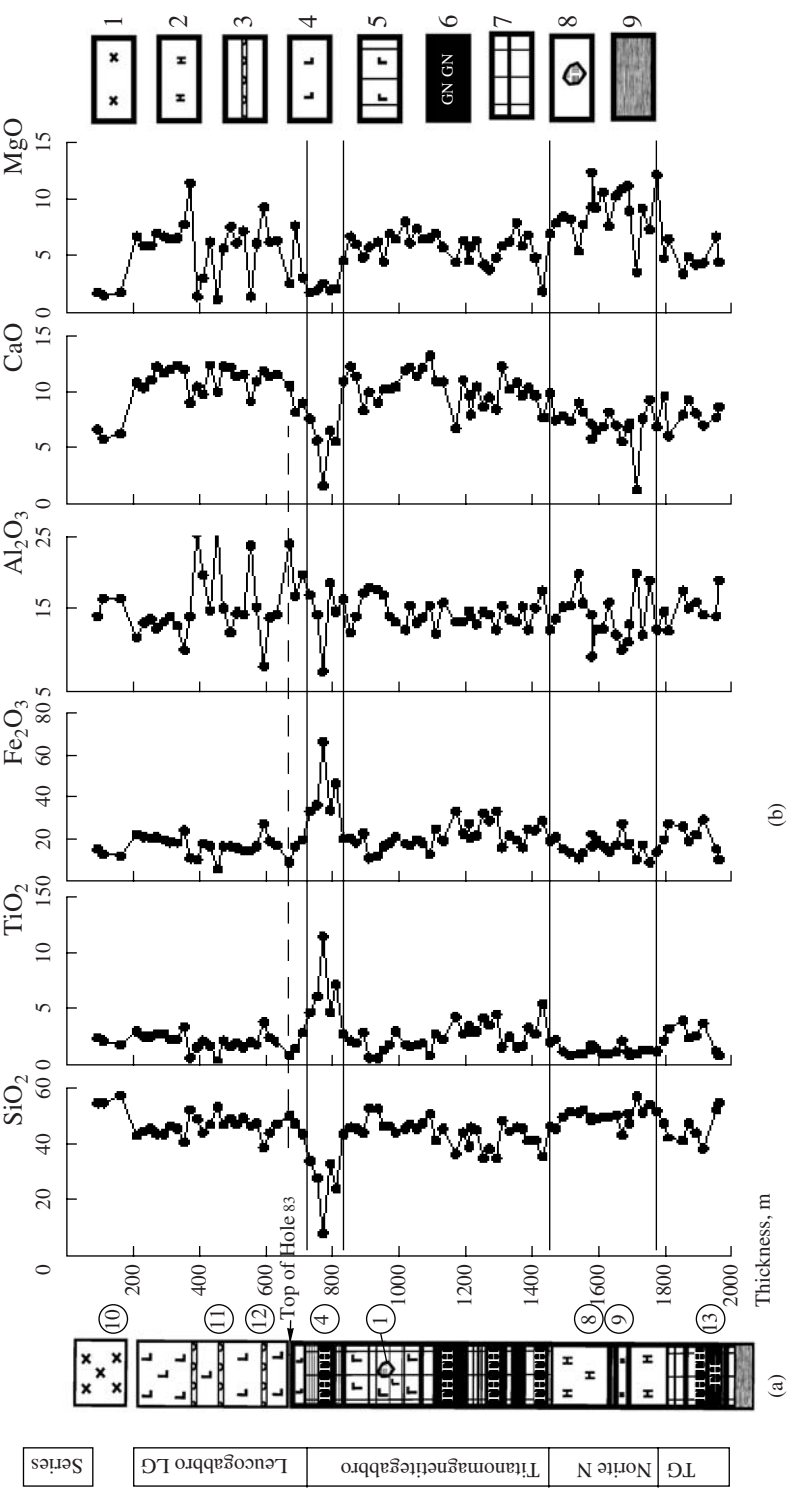

Fig. 4. Vertical section of the Chineiskii Massif (prepared based on materials recovered by Hole 83 and collected at exposures between its top and the apical surface). (a) Geological column (shows relative thickness in m); (b) distribution of major oxides (concentrations are in wt %). Circled numerals show the petrochemical types of rocks distinguished by cluster analysis: (1) monzodiorites and quartz diorites, (2) norites, (3) anorthosites, (4) leucogabbro, (5) gabbro and gabbronorites, (6) titanomagnetite ores, (7) titanomagnetite gabbronorites, (8) pyroxenite xenolith, (9) host rocks of the Udokan Group. White beds are gabbro in the titanomagnetite gabbro series and norites in the norite series.

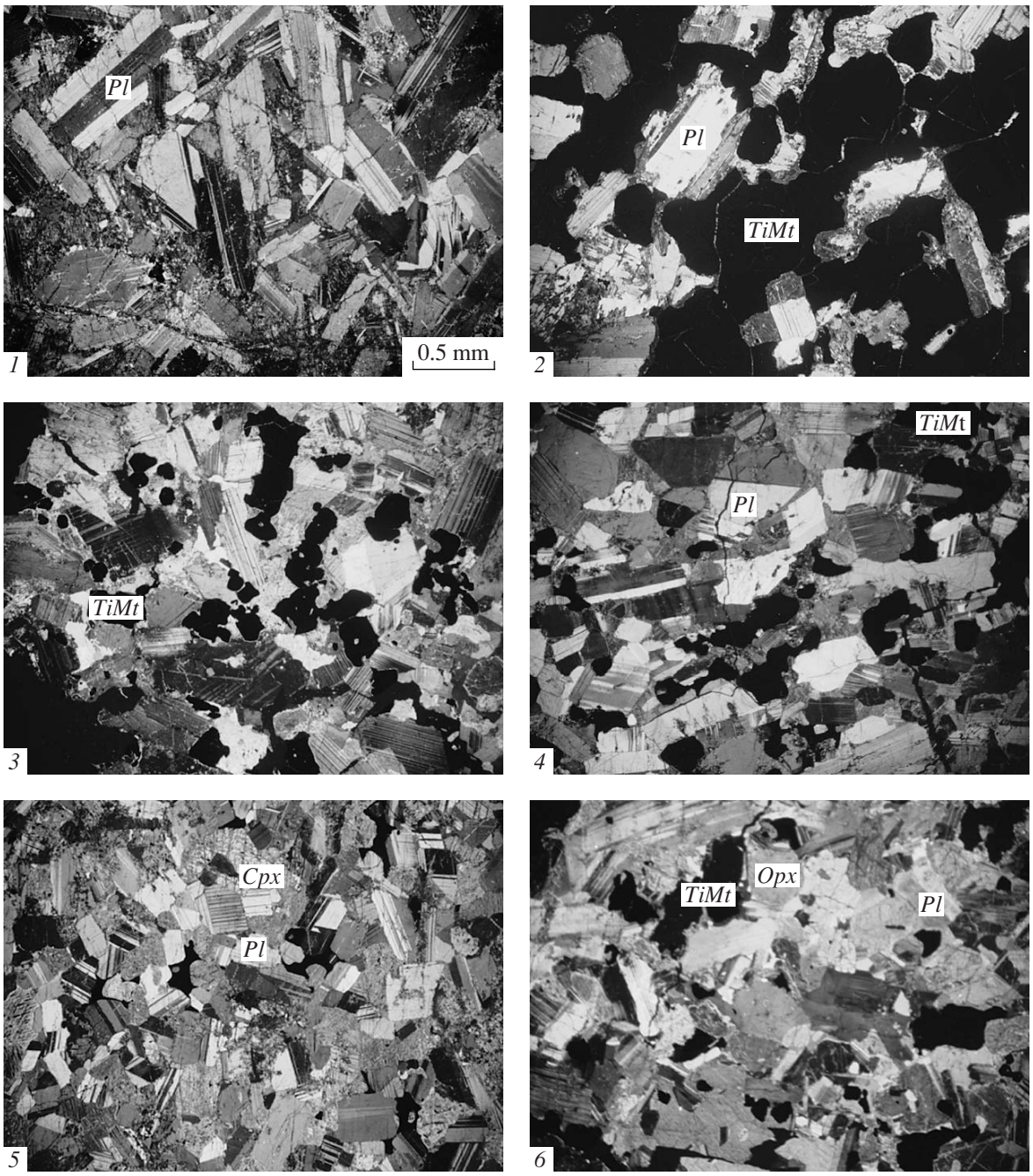

Fig. 5. Photographs of major rock types from the Chineiskii Massif: (*1*) anorthosite; (*2*) chinite; (*3*) titanomagnetite leucogabbro; (*4*) titanomagnetite gabbronorite with a trachytoid texture; (*5*) gabbronorite; (*6*) norite. All photographs are on the same scale.

centrations of eight major oxides: SiO_2, TiO_2, Al_2O_3, FeO_{tot}, MgO, CaO, Na_2O, and K_2O.

Rock complexes were clustered based on the chemical analyses of selected samples from a reference vertical section in the western block of the intrusion, with the sampling sites spaced 20 m apart (along Hole 83 for the lower part and in exposures at the surface for the upper part; Tables 2, 3). We also used data on rocks from the eastern part of the pluton, which were not found in the western block. The overall dataset also included analyses of rocks from Hole 11 from [32], in which total FeO (XRF analyses for all of these and the other samples), Fe^{2+}, and Fe^{3+} were determined. As a result, the overall number of rock compositions in the dataset amounted to 216. The results of their systematic hierarchical grouping are displayed in the form of a tree diagram in Fig. 8.

It is important to mention that the clustering procedure does not involve any formal criterion for the subdivision of the composition dataset into types or groups

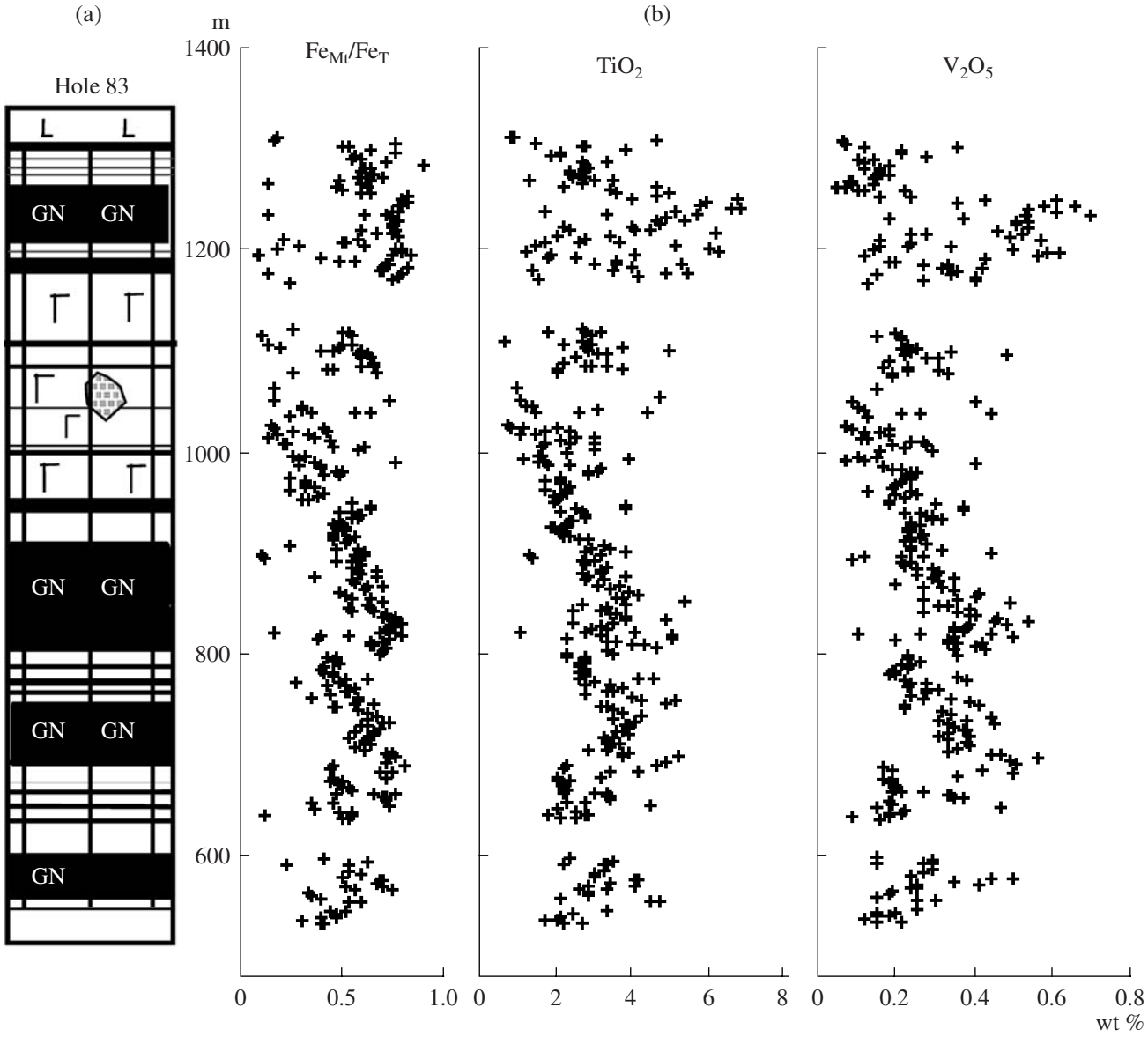

Fig. 6. Variations in the ratio of magnetite Fe to the total Fe in rocks, TiO_2, and V_2O_5 in the vertical section of the titanomagnetite gabbro series. (a) Geological column (Hole 83); (b) distribution of major oxides (wt %). See Fig. 4 for symbol explanation.

(no numerical level for grouping is specified), and this procedure can be conducted based on the structure of the tree diagram, regardless of the information, including any structural–petrographic and geological data [37]. In classifying the rocks of the Chieiskii Massif, we proceeded from the structure of the tree diagram, which successively groups the compositions (Fig. 8) and controlled the consistency between the distinguished types and described petrographic types. Thus we recognized 13 persistent petrochemical types (Table 4), which allowed us to reveal the finer structure of the distinguished four rock groups.

The tree diagram (Fig. 8) shows the most distinct individualization of the first rock type, which comprises pyroxenite xenoliths (group I according to geological data). The diagram also displays clearly recognizable rocks of plagioclase–titanomagnetite composition, which were referred to as chinites (type 4, average FeO concentration close to 59 wt %) and occur in the leucogabbro series. Rock types 11, 12, and 13 are closely similar, and their differences are controlled by variations in the relative amounts of titanomagnetite in the leucogabbro. These rocks were found in both the leucogabbro series and in the upper part of some rhythms in the titanomagnetite gabbro series (group II). Significant similarities were also displayed by types 5, 6, and 7, which represent gabbroids with relatively insignificant variations in the contents of their major rock-forming minerals: pyroxenes, titanomagnetite, and plagioclase. All of them are classed with the titano-

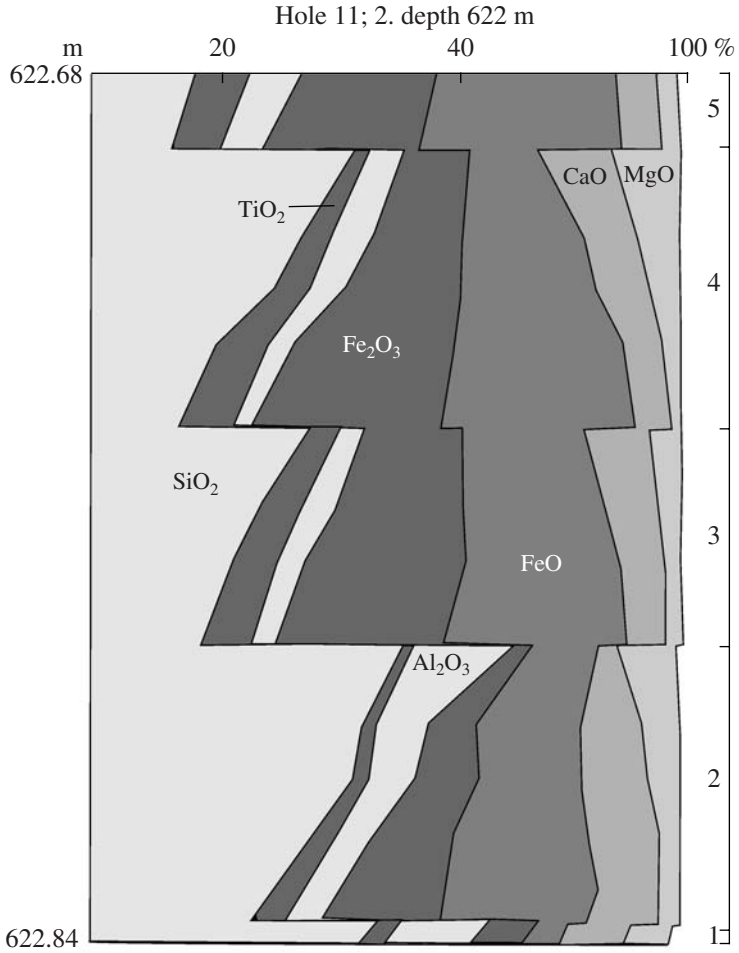

Fig. 7. Variations in the contents of major oxides in the vertical section of microrhythms in the lower part of the titanomagnetite gabbro series (rock group II). Numerals mark discrete rhythms.

magnetite gabbro series and characterize various parts of the rhythmic units. Types 2 and 3, as well as 8 and 9, typically contain minor amounts of orthopyroxene: rocks of this composition are stratigraphically predominant in the norite series (group III, types 8, 9) but were also found in the lower part of the titanomagnetite gabbro series (group II, types 2, 3). The rocks of type 10 significantly differ from all others and are monzodiorites from the upper and marginal eastern parts of the massif (group II).

All of the recognized types are thus consistent with the petrographic varieties of rocks of the Chineiskii pluton (groups I–III) and generally exhibit an unsystematic distribution in the vertical section of the intrusion (Fig. 4). Only some of them occur at certain stratigraphic levels (Fig. 4): type 4 chinites are localized at the boundary between the titanomagnetite gabbro and leucogabbro series, types 11 and 12 occur in its central part, and types 8 and 9 are typical of norite series and 1 type (xenoliths of group I) is restricted to the upper part of the titanomagnetite gabbro series.

The rock types distinguished by cluster analysis likely correspond to a certain differentiation stage of the parental magma of the pluton, which allowed us to formulate the task of reproducing the phase and chemical characteristics of this source and less primitive (residual) magmas. These problems were solved by numerical simulation of melt–crystal equilibria [40].

CALCULATION OF THE TEMPERATURE AND COMPOSITIONS OF THE CHINEISKII MAGMAS

In order to evaluate the temperatures and compositions of magmas from which the rocks of the Chineiskii intrusion crystallized, we utilized the results of simulation of the equilibrium crystallization of melts corresponding to the compositions of rocks of various petrochemical types (Table 4). This technique is a variant of the geochemical thermometry of intrusive basites [41], which is underlain by the analysis of the temperature–composition trends of modeled liquids and data on the composition of the major rock-forming minerals. The

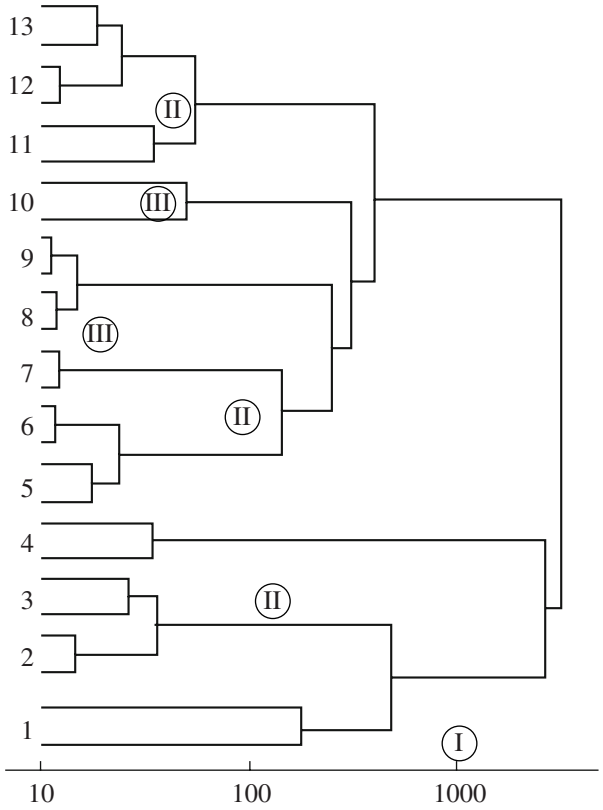

Fig. 8. Tree diagram showing the result of the successive clustering of rocks of the massif into stable petrochemical groups.

The diagram shows a fragment of a general tree diagram for the formal degree of geochemical differences of the rock collection >10. Roman numerals denote major rock types, and Arabic numerals show their petrochemical types.

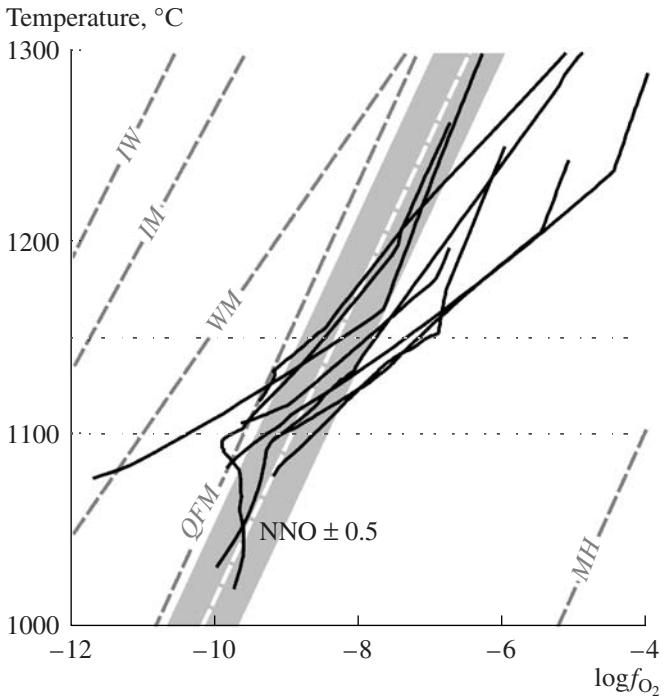

Fig. 9. T-log f_{O_2} diagram with the results of simulations of the equilibrium crystallization of melts corresponding to representative rocks of the Chineiskii Massif (Table 4). Solid lines characterize the evolution of the modeled melts with regard for the specified Fe_2O_3 and FeO concentrations (the system is closed with respect to oxygen). Dotted lines show the temperature range of the calculated cotectics with olivine + plagioclase ± magnetite ± clinopyroxene. The overlap area of these characteristics (shaded) corresponds to the probable redox parameters at which the Chineiskii magma crystallized (NNO ± 0.5).

calculations were aimed at the evaluation of the chemical compositions of the melts that were in equilibrium with the mineral phases in various rock types.

Simulation conditions. The thermodynamic simulations can be carried out based on independent data on the pressure, concentrations of volatile components, and redox conditions under which the magmatic melts crystallized. The low alumina contents in the Chineiskii orthopyroxene (0.8–1.3 wt % Al_2O_3) suggest that the massif was emplaced at a shallow depth, at a pressure no higher than ~1.5 kbar (see the McGregor diagram in [18]). The absence of primary magmatic hydroxyl-bearing minerals from the major rock types testifies that the parental magmas were undersaturated in H_2O, which led us to suggest that the water concentrations in the melts were (under the aforementioned pressures) likely no higher than ~0.5 wt %. This warrants calculations at nominally dry conditions and a total pressure P = 1 kbar. To evaluate the redox parameters of magma evolution under these conditions, we provisionally simulated the equilibrium crystallization of the melts of eleven representative rocks, whose Fe^{3+}/Fe^{2+} ratios were analyzed (Table 5). The results of these simulations by the COMAGMAT-3.5 [39] computerized model allowed us to constrain the probable temperature range of the melts, which was evaluated at 1100–1150°C. The redox conditions of crystallization of all rock types were proved to be close to the NNO ± 0.5 buffer equilibrium (Fig. 9). The calculated parameters were then used for simulations with the recognized 13 petrochemical types. These simulations were carried out successively by means of increasing the crystallinity of the system at a step of 1 mol % and were terminated at a high crystallinity of the modeled systems at 65–90% crystalline phases.

Simulation results. The modeled crystallization sequences of the melts of the major rock types are shown in Fig. 10[1]. The rocks are characterized by the presence of olivine, which was the first phase to crystallize in five instances (types 1–3, 8, and 9) and was also detected in five other cases on the cotectic lines,

[1] We do not show here data on type 4 because of the extremely high Fe concentration (Table 3), which resulted in the long-lasting crystallization of magnetite alone under conditions extending beyond the calibration range of the COMAGMAT-3.5 system.

Table 4. Petrochemical rock types distinguished in the Chineiskii Massif based on the results of cluster analysis

Type	Group	Series	SiO_2	TiO_2	Al_2O_3	FeO	MnO	MgO	CaO	Na_2O	K_2O	P_2O_5
1	1		45.3	1.37	4.15	20.27	0.22	13.44	14.62	0.37	0.2	0.05
2	2	TMG	45.69	2.53	8.72	24.77	0.27	5.84	2.51	1.23	0.16	0.05
3	2	TMG	37.04	4.47	7.43	34.28	0.27	9.5	5.61	1.06	0.29	0.01
4	2	TMG	16.49	9.17	4.98	59.34	0.27	5.84	2.51	1.23	0.16	0.02
5	2	TMG	46.5	2.08	14.13	15.19	0.17	6.21	11.13	3.03	0.72	0.08
6	2	TMG	44.39	2.49	12.58	18.46	0.2	7.26	11.64	2.5	0.43	0.05
7	2	TMG	46.8	1.98	15.23	16.98	0.15	5.88	10.15	2.3	0.45	0.08
8	3	N	49.57	1.36	13.1	16.2	0.2	9.72	6.82	2.32	0.65	0.07
9	3	N	52.75	0.84	16.32	11.35	0.17	7.59	7.63	2.63	0.65	0.07
10	2	LG	52.31	1.75	14.83	13.88	0.2	5.52	6.1	2.66	2.4	0.35
11	2	LG	51.04	0.91	23.68	7.54	0.09	1.45	10.36	4.01	0.78	0.13
12	2	LG	45.89	2.34	18.77	17.34	0.14	2.33	9.47	3.17	0.46	0.08
13	2	TMG	36.37	4.59	16.25	27.9	0.14	2.88	7.76	3.25	0.51	0.05

Note: (1) Rock series: TMG—titanomagnetite gabbro, LG—leucogabbro; N—norite; (2) oxide concentrations are given in wt %.

Table 5. Representative analyses of rocks of various petrochemical types (with measured concentrations of P_2O_5 and Fe_2O_3)

no.	Type	Sample	SiO_2	TiO_2	Al_2O_3	Fe_2O_3	FeO	MnO	MgO	CaO	Na_2O	K_2O	P_2O_5	LOI	Total
1	1	58012500	44.17	1.36	4.23	3.86	17.78	0.23	13.48	13.68	0.46	0.25	0.02	0.07	99.59
2	2	11622840	46.64	2.25	7.79	7.85	17.1	0.29	11.21	6.06	1.31	0.43	0.04	0.02	100.99
3	3	11622730	36.1	4.61	6.93	15.11	19.8	0.29	8.96	7.89	0.96	0.26	0.03	0.03	100.97
4	4	11063800	16.53	8.58	4.42	30.74	28.45	0.23	7.04	2.38	0.64	0.12	0.02	0.31	99.46
5	6	11020400	42.4	2.12	13.2	10.13	10.34	0.17	6.29	11.88	2.7	0.38	0.03	0.25	99.89
6	7	11013800	45.89	1.02	17.87	4.85	9.23	0.02	6.77	10.77	2.36	0.23	0.17	0.18	99.36
7	8	11089500	50.96	0.95	14.98	3.14	10.02	0.17	8.8	7.44	2.19	0.67	0.07	0.27	99.66
8	9	11092050	48.55	1.45	9.69	4.88	9.27	0.18	9.61	13.37	1.76	0.57	0.09	0.37	99.79
9	11	11029500	48.84	1.25	22.48	2.08	7.95	0.11	1.45	10.16	3.42	0.56	0.14	0.39	98.83
10	12	11053260	45.79	2.28	20.34	6.74	8.84	0.12	1.95	8.83	3.12	0.46	0.1	0.84	99.41
11	13	11045860	37.88	5.89	18.83	5.29	19.45	0.14	0.91	7.12	2.7	0.37	0.07	0.49	99.14

Note: (1) Sample numbers: the first two digits correspond to the hole number, and the third, through eighths digits correspond to the depths (in cm); (2) types correspond to the petrochemical types of rocks (Table 4); (3) oxide concentrations are given in wt %; LOI means lost on ignition.

together with plagioclase, pyroxene, and magnetite. The crystallization sequences for types 2, 3, 8, 9, 12, and 13 show that olivine occurs in reaction relations with the melt and completely dissolves due to a peritectic reaction and is replaced by pyroxenes and magnetite at $T =$ 1110–1150°C. Plagioclase did not crystallize in the monzodiorites (type 10). These observations indicate that the initial melts were saturated or weakly oversaturated with SiO_2, whose concentrations in the intercumulus system were also high. The oversaturation with SiO_2 controlled the crystallization evolution toward the *Ol*/*OPx* reaction point. The peritectic reaction in the cumulus–intercumulus–liquid system was responsible for the absence of modal olivine and the wide occurrence of norite among the rocks of the massif.

The modeled crystallization sequences of the rocks can be subdivided into two types. One of them is the "high-Al" type, which is typical of "leucogabbro" compositions and is characterized by the presence of a magnetite–plagioclase cotectic (petrochemical types 6, 7, 11–13). This type is characterized by the early crystallization of plagioclase (at > 1250°C) and magnetite (close to 1200°C). The highest crystallization temperatures of magnetite (1365°C) were determined for chinites (types 4) and adjacent rocks of type 3 (1252°C), which have the highest Fe concentrations (59.3 and 34.3 wt % on average). These features and the similar crystallization temperatures of augite as the third cotectic phase (1108–1112°C) permitted us to combine the compositions of types 4, 11, 12, and 13 into a group of plagioclase–magnetite cumulates (which is consistent

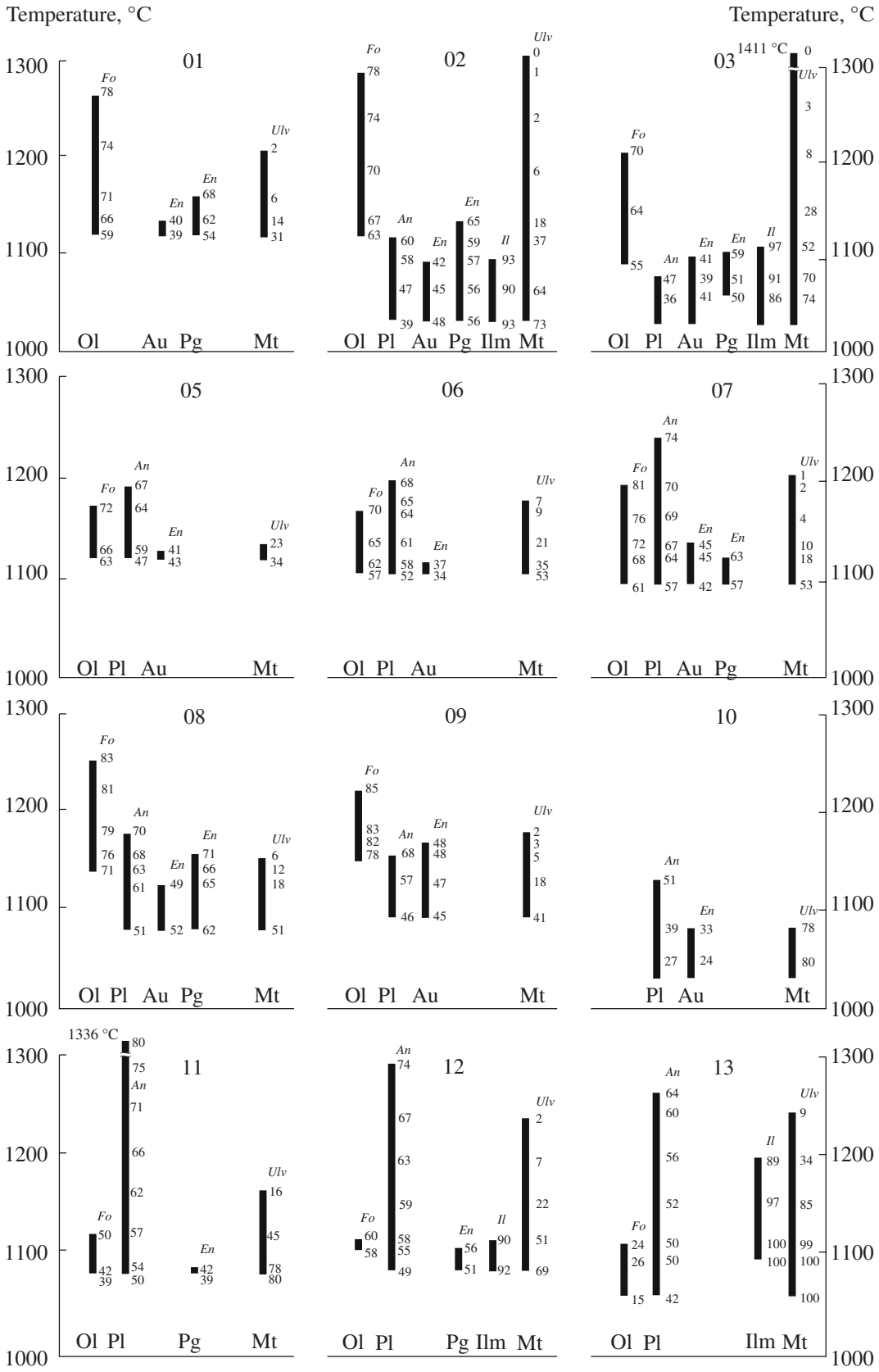

Fig. 10. Crystallization sequences and temperatures and the compositions of major minerals for various petrochemical rock types of the Chineiskii Massif. Numerals 01 through 13 mean the compositions of the petrochemical types in Table 5. Numerals near the crystallization lines of minerals demonstrate the dependence on temperature.

Table 6. Crystallization temperatures of melts determined based on the composition of minerals from the rocks

Petrochemical type	Measured compositions (mol %) of minerals			Crystallization temperature		Composition (mol %) of simulated crystals at specified temperatures							
						Cpx					*Opx*		
	An	*Opx*	*CPx*	ΔT, °C of crystallization	T_{mean}	*Fo*	*An*	*En*	*Fs*	*Wo*	*En*	*Fs*	*Wo*
1	–	–	44–48, *Wo*	1147–1124	1135	–	70.6	44	17	38	64	26	9
2	–	29–42, *Fs*	–	1119–1122	1120	–	–	–	–	–	58	38	4
3	–	29–32, *Fs*	–	1097–1086	1092	–	–	44	20	35	59	32	10
5	–	–	38–42, *En*	1128–1124	1126	65	57	41	16	43	–	–	–
6	54–58	–	–	1118–1122	1120	65	56	41	16	43	–	–	–
7	52–56	–	–	1103–1092	1098	–	54	45	21	34	58	33	9
8	50–60	–	–	1126–1110	1118	62	58	–	–	–	60	32	8
9	57–59	–	–	1100–1114	1107	–	58	47	21	32	60	32	8
10	44–47	–	–	1072–1087	1080	–	45	53	19	28	–	–	–
11	47–57	–	–	1142–1030	1136	–	57	–	–	–	–	–	–
12	54–57	–	–	1126–1114	1120	–	56	–	–	–	–	–	–
13	50–52	–	–	1135–1100	1128	–	53	–	–	–	–	–	–

Note: *An*—anorthite; *Cpx*—clinopyroxene, *Opx*—orthopyroxene, *Fo*—forsterite, *En*—enstatite, *Fs*—ferrosilite, *Wo*—wollastonite; *T* is the range of the crystallize temperatures of the mineral.

with petrographic observations), which may have been produced during close differentiation stages of the Chineiskii magmas. In this situation, the differences between the temperature at which plagioclase and magnetite appeared on the liquidus can be explained as a result of variations in the proportions of these minerals in the cumulus.

The second type of the modeled sequences can be referred to as magnesian and is characterized by the early cotectic crystallization of olivine with magnetite and olivine with plagioclase. This type includes petrochemical types 1–3, 8, and 9, with types 8 and 9 being the most primitive and representing the norites with a highly magnesian composition of the early liquidus olivine (Fo_{83} and Fo_{84}, respectively). The liquidus temperatures of these melts are 1230–1250°C, and their third crystallizing phase (at a temperature of approximately 1150°C) is augite or low-Ca pyroxene.

In compositions 1–3, plagioclase is a late phase and crystallizes at temperatures below 1110°C. This makes these compositions different from primitive types 8 and 9, in which plagioclase appears at 1160–1180°C. A type similar to these compositions is type 5, which is characterized by the concurrent crystallization of olivine and plagioclase within the same temperature range. During late crystallization stages, these minerals are accompanied by magnetite and augite (1140–1125°C).

The simulation results were utilized to evaluate the temperatures and compositions of the melts for various petrochemical rock types by the method described in much detail in application to the Skaergaard, Kiglapate, and Talnakh intrusions [41]. The method is underlain by the successive "fitting" of the modeled melts for each of the starting composition in search for liquids (in composition–temperature space) that could be in equilibrium with the mineral assemblage close to those of the rocks. This implies the comparison of the real and modeled compositions of the mineral phases and makes it possible to evaluate the melt temperatures accurate to 10–20°C for each of the petrochemical types. These problems were solved using representative microprobe analyses of plagioclase and pyroxenes from samples characterizing certain petrochemical types (Table 6). The temperature range thus constrained was usually no wider than 20°C: for example, it was 1110–1126°C for plagioclase composition within the range $An_{50–60}$. These calculation results were then analyzed using the average temperature values for each type and the compositions of the residual melts corresponding to these average temperatures (Table 7). In contrast to the previous table, this one is rearranged according to the calculated temperature decrease. This representation implies that the evolution of the liquid part of the magma during its solidification and differentiation was controlled by crystallization. In addition, Table 6 exhibits calculated amounts of cumulus phases in equilibrium with a given melt.

The values thus obtained point to a relatively narrow range of the crystallization temperatures of the Chineiskii magmas: 1140–1080°C (Fig. 11). The modeled melts are prone to gradually become depleted in MgO and CaO and enriched in SiO_2 and alkalis, which testifies to the occurrence of a fractionation trend from basalt to dacite. It is also worth noting the high FeO and TiO_2 concentrations (close to 3 wt % on average),

Table 7. Melt compositions simulated for the major petrochemical rock types

Type	*T*, °C	Sol. phase, %	*Ol*	*Pl*	*Au*	*Pg*	*Ilm*	*Mt*	SiO_2	TiO_2	Al_2O_3	FeO	MgO	CaO	Na_2O	K_2O	P_2O_5
11	1136	58	–	57	–	–	–	1	50.19	2.43	14	16.15	3.98	7.86	3.32	1.83	0.24
1	1135	35	9	–	–	26	–	–	50.85	2.43	12.71	15.68	5.28	10.15	1.62	0.92	0.23
5	1126	34	7	22	3	–	–	2	47.73	2.66	12.13	17.09	4.72	10.62	3.45	1.27	0.15
6	1120	36	9	23	–	–	–	4	47.02	3.15	11.16	17.89	4.98	11.59	3.1	0.83	0.11
2	1120	44	1	–	–	33	–	10	58.18	3.09	11.13	18.41	3.42	3.43	1.8	0.23	0.07
12	1120	58	–	48	–	–	–	10	49.81	3.35	11.93	17.79	4.04	9.06	2.84	0.82	0.16
8	1118	57	–	30	2	22	–	3	52.91	2.36	13.26	15.29	4.03	7.34	3.02	1.41	0.17
9	1107	73	–	15	52	–	–	7	56.98	2.02	14.06	12.78	3.16	5.67	2.94	1.89	0.24
7	1098	85	6	50	13	9	–	7	55.75	2.85	12.83	14.12	3.18	6.53	2.98	1.31	0.26
3	1092	46	–	–	15	2	5	25	59.66	3.34	12.52	12.45	2.23	5.01	3.35	1.06	0.38
10	1080	18	–	15	1	–	1	1	62.92	1.5	16.78	5.98	1.56	2.58	3.64	4.24	0.64
IM	1130	–	–	–	–	–	–	–	49.37	2.88	12.12	17.02	4.44	9.65	3.1	1.08	0.15

Note: (1) (1)–(3) and (5–12)—Simulated compositions of the petrochemical types;
(2) IM is the initial melt of the Chineiskii Massif (calculated as an average of simulated melt types 5, 6, 8, and 12);
(3) oxide concentrations (wt %) in solid phases;
(4) Sol. phase is the total amount of crystals in melt, including: *Ol*—olivine, *Pl*—plagioclase, *Au*—augite; *Pg*—pigeonite, *Ilm*—ilmenite, and *Mt*—magnetite.

which emphasize the ferrobasaltic character of the magmas that produced the rocks of the Chineiskii intrusion. The absence of clear-cut monotonous trends in the variation diagrams was caused by difficulties with the calculation of phase equilibria in the presence of high amounts of magnetite at temperatures close to 1100°C [40] and the possibility of the emplacement of initial melts of similar temperature but different phase composition. This is a likely reason for the individualized position of composition 10 (1080°C), which was produced by the equilibrium crystallization of monzodiorite (Fig. 11).

The data on the phase composition presented in Table 7 and Fig. 11 suggest that the parental magmas of the Chinneiskii pluton included a melt containing 4–5 wt % MgO and were characterized by similar emplacement temperatures (close to 1130°C). These parameters are characteristic of the melts of petrochemical types 5, 6, 8, and 12. For these four compositions in Table 7, we calculated the average composition of the initial melt corresponding to the liquid constituent of the magma (or magmas) that filled the chamber of the Chinneiskii pluton. Figure 11 shows the fractionation trajectory of this melt calculated by the COMAGMAT model at the same physicochemical parameters at which the temperature calculations were conducted. The calculated lines of fractionation crystallization generally coincide with the compositional trends of the modeled liquids for various petrochemical types. This can be regarded as evidence for genetic relations between the rock types and the plausibility of our temperature estimates and the calculated composition of the parental Chineiskii melt (in spite of the provisional character of our calculations). A more accurate evaluation of the proportions melt and solid phases in the "magmas" of the blocks is hampered by the lack of reliable data on the average composition of the major structural units of the Chineiskii pluton.

TRACE ELEMENTS IN THE ROCKS

The conclusion that the parental magmas of the Chineiskii intrusion had a ferrobasaltic composition puts forth the problem of the nature of the source from which the recognized initial and derivative parental melts were derived. This problem is considered from the geochemical viewpoint with regard for the primitive mantle-normalized trace-element patterns of the rocks composing the massif. The patterns can be classified into three types (Table 8, Fig. 12). The first of them is typical of rock groups II and III (titanomagnetite gabbro, leucogabbro, and norite series), which dominate in the intrusion. The second type is characteristic of the rocks of marginal facies: quartz diorites, monzodiorites, and the lamprophyres of group IV. The third vari-

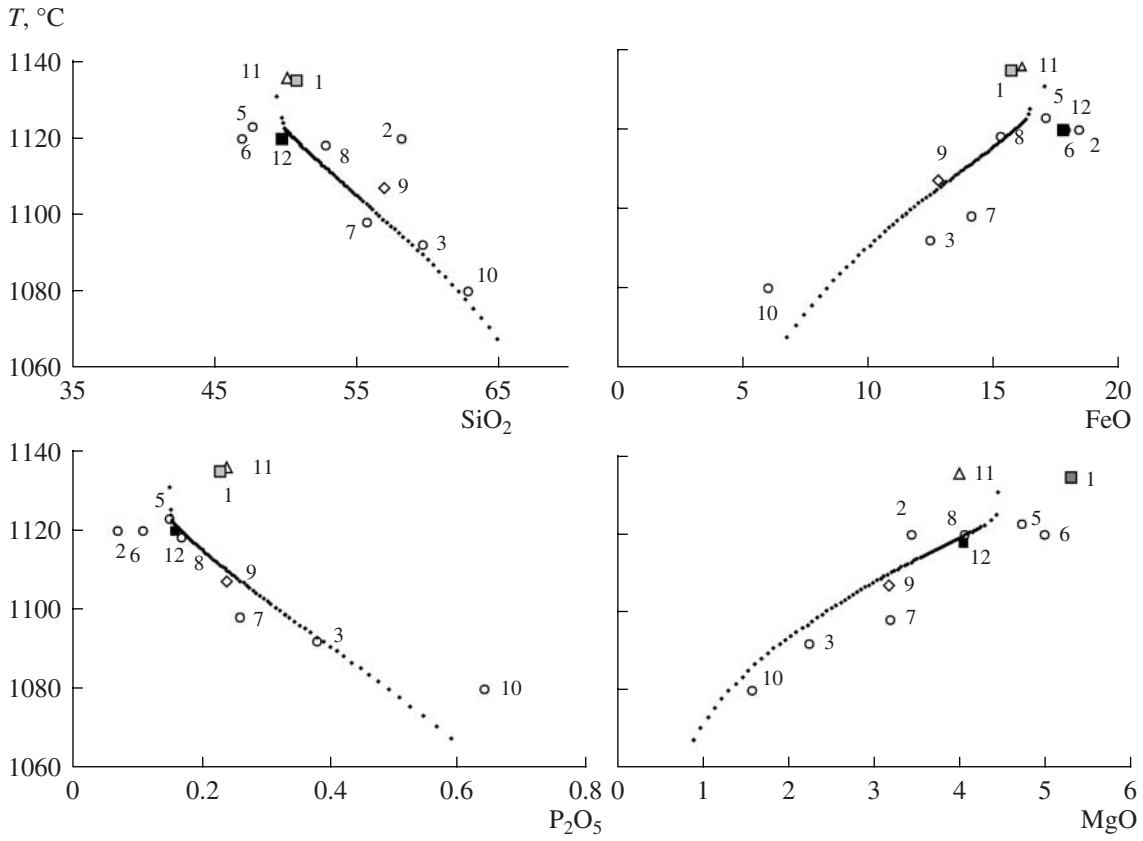

Fig. 11. Crystallization fractionation trends for the modeled melt of the Chineiskii Massif and the compositions of the modeled melts of the major petrochemical types (numerals). 1—Corresponding to the major rock types (Tables 6, 7): gray square corresponds to pyroxenites, type 1 (sample 0301, rock group I); diamond—gabbronorites, type 9 (sample 0303, rock group III, gabbronorite series); triangle—titanomagnetite-bearing leucogabbro, type 11 (sample 0304, group II, leucogabbro series); black square—titanomagnetite-bearing leucogabbro, type 12 (sample 0307, group II, titanomagnetite gabbro series); 2—circles correspond to other petrochemical types (numbers correspond to those in Table 6).

ety of the patterns characterizes the pyroxenites of group I.

Similarities between the trace-element patterns of the two major groups suggests genetic relations between these rocks of the massif (samples 0303, 0304, 0306, and 0307) and their affiliation with the differentiation products of the parental magma. The structure of these patterns is typologically close to those of the continental crust, which are characterized by high concentrations of incompatible elements (a steep slope of the left-hand segment, whose $(La/Sm)_N$ ratio varies from 3.1 to 4.3) and the presence of negative Ta–Nb anomalies, positive Pb anomalies, and strong positive Ti anomalies. Only the patterns of rocks of the norite series are devoid of the latter, which can be logically explained by the low contents of Fe–Ti oxides. The aforementioned features of the trace-element patterns make these rocks principally different from MORB, OIB, and other mantle derivatives [43, 44]. The gentle slope of the right-hand parts of the patterns, which are characterized by low $(Gd/Yb)_N$ = 1.5–1.7, accentuates the geochemical specifics of the parental magmas of groups II and III of the rocks and suggests that the source from which the initial magmas were derived contained no garnet.

The higher degree of the accumulation of incompatible elements (samples 0321/1) in the marginal facies and lamprophyres (rock group IV) can be explained by the differentiation of the parental magmas with the origin of relatively enriched residual melts. This likely explains the main difference of the second-type patterns, which are characterized by the absence of positive Ti anomalies and the presence of weakly pronounced Ti minima in the patterns. Such relations are typical of magma evolution associated with magnetite crystallization. The patterns of the pyroxenites (group I, samples 0301, 2101/2, and 0302) are more different. These rocks are depleted in LREE ($(La/Sm)_N$ varies from 0.99 to 1.12) and have relatively low concentrations of trace elements. Their REE patterns are nearly horizontal and close to those of the primitive mantle. The pyroxenites show practically no Ta–Nb minima but have clearly pronounced Sr anomalies, perhaps, because of low plagioclase contents in these rocks. The typology of the patterns is largely controlled by the nearly monomineralic composition of the rocks. These

Table 8. Representative major- and trace-element compositions of rocks from the Chineiskii Massif

Component	O301	2101/2	O302	O303	O304	O305	O306	O307	O321/1	O308
	Petrochemical rock types									
	1	1	1	9	12	10	7	12	10	–
SiO_2	47.54	41.83	43.62	53.54	46.38	55.78	45.5	45.87	53.28	56.03
TiO_2	1.24	2.72	1.96	0.71	2.47	1.14	3.17	2.50	2.38	1.04
Al_2O_3	4.85	4.42	1.76	15.37	17.11	17.15	16.06	21.08	13.81	18.21
Fe_2O_3	10.62	26.99	24.35	10.88	17.27	9.35	17.28	14.40	14.61	7.54
MnO	0.17	0.32	0.29	0.18	0.17	0.13	0.16	0.11	0.23	0.14
MgO	11.62	11.22	15.46	7.76	3.76	2.07	3.68	1.74	1.61	4.21
CaO	21.02	12.17	11.27	7.15	8.26	7.80	9.62	9.58	6.50	8.14
Na_2O	0.08	0.26	0.16	2.63	3.40	3.75	3.16	3.54	3.79	2.86
K_2O	0.01	0.16	0.02	0.63	0.60	1.49	0.42	0.33	1.68	1.25
P_2O_5	0.012	0.07	0.006	0.08	0.10	0.13	0.08	0.033	0.69	0.25
Cr_2O_3	0.011	0	0.028	0.014	0.014	0.004	0.01	0.01	0.002	0.014
LOI	2.52	0.24	0.63	0.36	0.11	0.23	0.18	0.27	0.7	0.17
Total	99.7	100.44	99.53	99.30	99.61	99.0	99.28	99.47	99.3	99.8
Li	9.8		6.5	5.6	6.3	9.5	5.4	4.2	9.2	21.6
Sc	47.2	99.4	83.4	19.1	25.0	22.9	16.1	17.2	28.4	21.1
Ti	7476	14754	10548	4175	12589	6228	17041	13734	11117	5711
V	725	989	2335	234	935	281	1675	1112	27.2	160
Cr	105	103	159	119	71.3	11.3	17.8	50.3	11.4	122
Mn	1339	2136	2145	1458	1109	888	1147	737	1525	838
Co	32.7	103	151	73.8	76.4	32.1	81.8	71.0	21.9	23.2
Ni	104	156	150	94.2	124	28.1	103	151	8.87	14.6
Cu	79.4	189	55.5	62.5	171	87.2	148	403	15.4	13.4
Zn	41.3	139	126	85.9	103	79.8	113	88.4	149	86.3
Ga	10.0	14.8	4.5	18.1	26.8	22.9	25.1	27.9	22.4	19.2
Rb	0.52	3.38	2.26	17.4	20.9	60.1	14.1	8.73	48.3	37.9
Sr	16.5	41.3	21.7	295	365	304	292	406	306	537
Y	13.6	22.6	8.97	10.6	10.6	23.1	11.1	5.01	33.6	22.4
Zr	55.1	32.3	18.3	52.9	51.5	143	44.9	24.0	115	93.3
Nb	1.85	1.94	2.89	2.66	3.03	6.60	2.76	1.58	9.03	9.35
Mo	0.31	0.69	0.41	0.38	0.44	1.26	0.57	0.32	1.75	0.73
Cs	0.04	0.20	0.12	0.66	0.64	1.33	0.51	0.29	1.52	1.44
Ba	14.2	43.0	16.5	255	298	524	220	200	611	538
La	3.7	7.35	2.29	10.1	13.6	24.7	9.02	6.01	31.8	28.7
Ce	10.7	17.1	7.2	20.7	22.6	50.2	18.6	10.8	76.6	60.6
Pr	1.63	2.42	1.15	2.40	2.65	5.83	2.19	1.21	8.94	7.36
Nd	8.08	11.6	5.55	9.62	10.2	22.0	8.79	4.74	36.0	29.1
Sm	2.15	3.09	1.49	1.91	2.00	4.31	1.83	0.94	7.31	5.44
Eu	0.43	0.91	0.26	0.66	0.87	1.25	0.72	0.65	2.54	1.67
Gd	2.36	3.39	1.60	1.79	1.85	3.82	1.78	0.82	6.69	4.47
Tb	0.39	0.55	0.25	0.29	0.29	0.60	0.28	0.12	0.98	0.65
Dy	2.41	3.48	1.57	1.78	1.68	3.57	1.71	0.81	5.74	3.65
Ho	0.47	0.72	0.33	0.38	0.35	0.74	0.36	0.16	1.16	0.73
Er	1.26	1.95	0.86	1.12	0.97	2.11	1.03	0.46	3.15	2.00
Tm	0.18	0.28	0.13	0.17	0.14	0.31	0.15	0.07	0.45	0.29
Yb	1.08	1.82	0.80	1.09	0.90	2.04	0.95	0.42	2.77	1.83
Lu	0.16	0.28	0.12	0.17	0.13	0.30	0.14	0.06	0.42	0.27
Hf	2.24	1.04	0.62	1.37	1.36	3.62	1.21	0.67	3.30	2.50
Ta	0.22	0.47	0.28	0.22	0.23	0.52	0.52	0.22	0.96	0.57
Pb	2.32	2.38	2.33	4.05	4.34	14.0	4.18	4.43	9.43	8.17
Bi	0.12	0.10	0.09	0.05	0.09	0.18	0.07	0.15	0.12	0.09
Th	0.54	1.85	0.36	2.57	2.25	7.89	2.24	1.12	6.50	3.80
U	0.17	0.27	0.11	0.75	0.73	2.12	0.51	0.31	2.17	0.94

Note: (1) Analyses were carried out by XRF (major components, given in wt %) at the Vernadsky Institute of Geochemistry and Analytical Chemistry, Russian Academy of Sciences, analysts I.A. Roshchina and T.V. Romashova and by ICP-MS (trace elements, given in ppm) at Institute of the Mineralogy, Geochemistry, and Crystal Chemistry of Rare Elements, analyst D.Z. Zhuravlev; (2) sample numbers: 0301, 2101/2, O302—pyroxenites, 0303—norite, 0304—leucogabbro, 0305, 0321/1—monzodiorites, 0306—titanomagnetite leucogabbro,O307—titanomagnetite gabbro, O308—gabbrodiorite from the Lukturskii Massif.

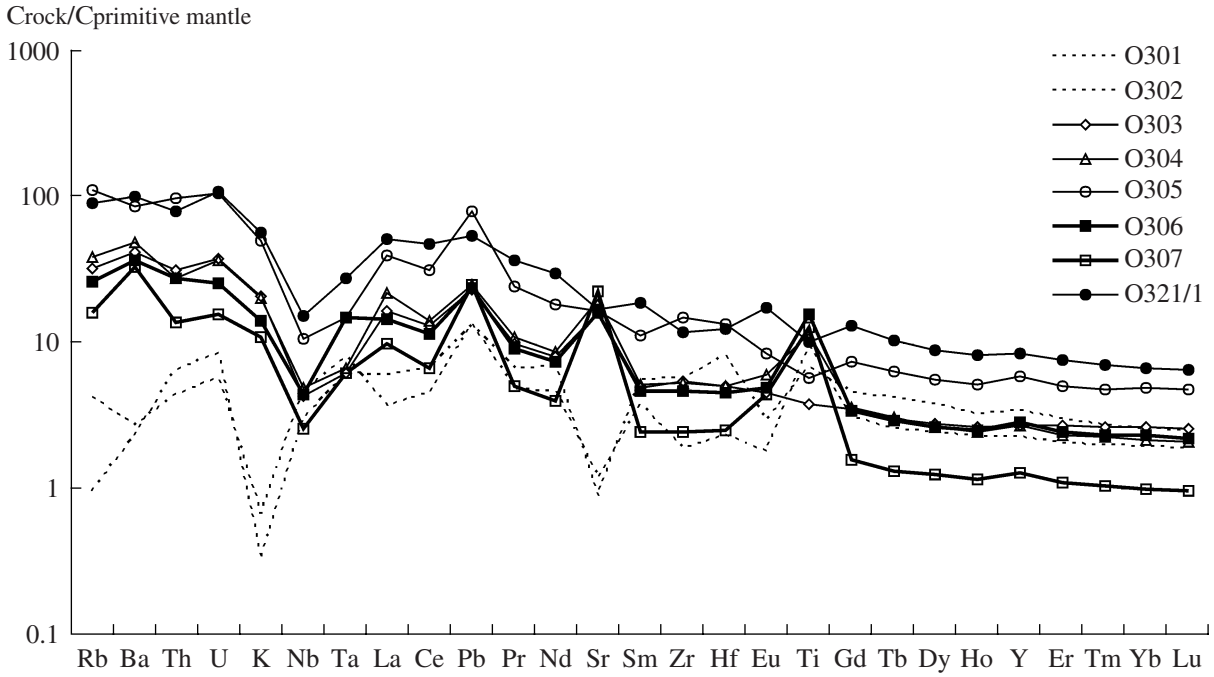

Fig. 12. Distribution of concentrations of K, Ti, and trace elements in rocks from the Chineiskii Massif normalized to the composition of the primitive mantle [42]. The numbers of patterns correspond to those of analyses in Table 8.

rocks are similar to those composing the bulk of the intrusion in having positive Ti anomalies and analogous HREE patterns (Fig. 12). The clinopyroxenites were likely produced by the differentiation of the most primitive magmas, because these rocks have the lowest concentrations of LILE (Cs, Rb, Ba, Sr, Rb, and K). They bear high concentrations of some HFSE (U and Th).

The REE patterns of the rocks composing the intrusion also testify that these rocks can be subdivided into four types (Fig. 13). Two of them are closely similar: these are the patterns of the rocks composing the bulk of the intrusion (the rocks of groups II and III). They are characterized by relatively low Gd/Yb ratios, which vary within narrow limits (from 1.86 to 2.06) for the rocks of group II and do not exceed 1.6 for the rocks of group III. Thus the REE patterns of the two major groups have slightly different slopes over HREE. Both groups are similar in having Eu minima.

The third type of the REE patterns has slopes and configurations generally similar to the aforementioned two but shows practically no Eu anomalies and is characterized by higher concentrations of all REE. This type of REE pattern is typical of the monzodiorites and lamprophyres of group IV, which shows certain similarities with the major rock varieties composing the intrusion.

Finally, the fourth type of the patterns is typical of the pyroxenites and xenoliths of rock group I. Similarly to the patterns of all trace elements, the REE patterns also differ from those of all other rocks. These patterns are depleted in LREE and include negative Eu anomalies.

At the same time, typological similarities between all of the patterns are obvious (if we ignore such elements as Sr and Eu, whose concentrations are largely controlled by variations in the contents of certain minerals in the rocks, first of all, plagioclase).

DISCUSSION

Recent advances in understanding the geology and petrology of classic layered plutons led to their regarding as intermediate chambers that are produced by mantle melts emplaced into the Earth's crust. They are usually thought to be the roots of volcano-plutonic systems with volcanic plateaus situated above magmatic reservoirs and connected with them via dike belts [45, 46]. The vertical amplitude of such systems amounts to a few kilometers, and only younger significant vertical tectonic motions brought these rocks to the surface and made them accessible for studying.

Many researchers reported geological data demonstrating the existence of such large magmatic systems. An example of a complex dispersed system is provided by the Koilismaa basite intrusion in Finland [47], which consists of a series of thin bodies interpreted as a part of a differentiated lopolith that was once single and was then disintegrated by faulting. Its deeper-seated constituent is the Njarjakavaara intrusion 50 km east of it. The bodies are connected by an unexposed "connecting dike" [30]. A somewhat different mechanism was pro-

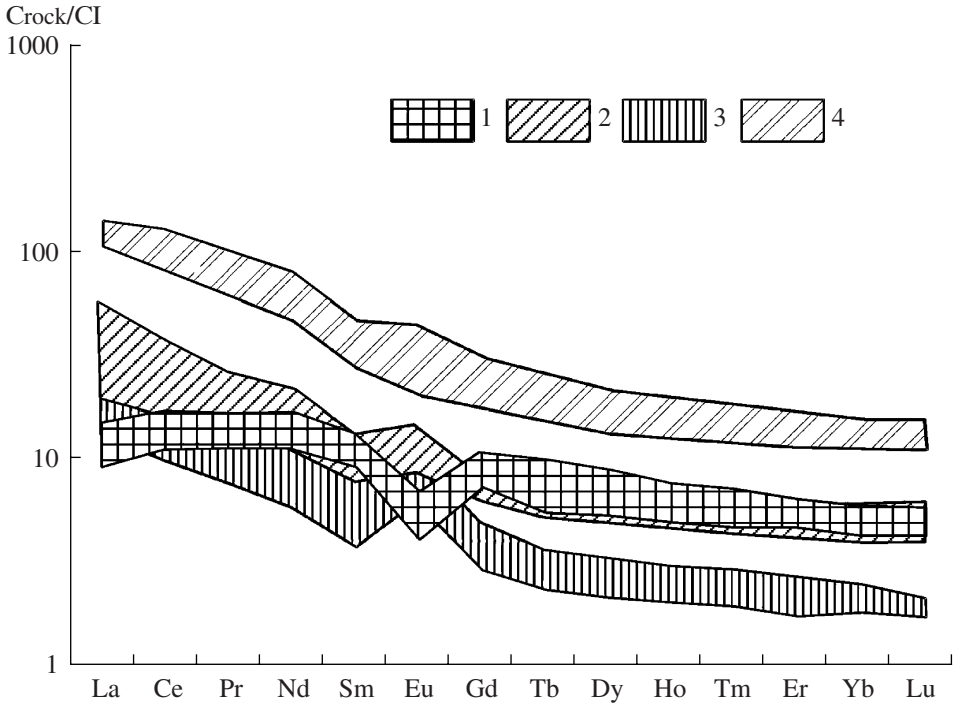

Fig. 13. Chondrite-normalized REE patterns of rocks from the Chineiskii Massif. (1) Pyroxenites, rock group I; (2) gabbronorites, rock groups II and III; (3) titanomagnetite gabbro, rock group II; (4) lamprophyres, rock group IV.

posed for the genesis of the Great Dike in Zimbabwe. This mechanism implies the occurrence of a series of subchambers, each with its own feeding system. The emplacement of fresh melt portions resulted in their connecting into a single system of the Great Dike [48].

The Kodar–Udokan district is another example of such a Proterozoic magmatic system of complicated structure in a crustal zone highly permeable to ultrabasic–basic melt. This zone developed at the boundary of the Siberia Platform and young foldbelts around it.

The unity of some of the layered massifs of the Chineiskii Complex (Chineiskii, Mailavinskii, and Lukturskii), gabbronorite dikes of the Chineiskii Complex, and separated exposures of gabbroids near the Lurbunskii granitoid massif is confirmed by the character and structure of the gravity and magnetic fields in the area.

Geochemical data on the rocks of some ultrabasite–basite bodies in the Kodar–Udokan district provide further evidence in support of genetic links between the magmatic bodies (Table 9). Figure 15 shows primitive mantle-normalized trace-element patterns of gabbroids from the Lukturskii Massif, Udokan Dike, and titanomagnetite gabbro from the Mailavskii Massif in comparison with the patterns of rocks from the Chineiskii Massif. To make the plots more illustrative, we subdivided them into two parts. Figure 15a demonstrates the identity of the patterns typical of the products of the most strongly fractionated melts: the monzodiorites of the Chineiskii intrusion, gabbronorites of the Lukturskii Massif, and the Udokan Dike. They are characterized by a significant enrichment in LREE and show Ti anomalies. Figure 15b displays the patterns of elements typical of rocks with elevated contents of titanomagnetite: titanomagnetite gabbro and gabbrodiorites from the Chineiskii Massif and titanomagnetite gabbro from the Mailavskii Massif. The high contents of oxide minerals in these rocks predetermined their lower concentrations of all trace elements, particularly LILE, and significant positive Ti anomalies. In spite of certain differences in the typology of the patterns, which were caused by the mineralogy of the rocks, all of these rocks are closely similar: all of them have similar slopes of both the right-hand and, particularly, the left-hand parts of the patterns and display clearly pronounced Ta–Nb anomalies in the absence of Th–U anomalies. These features point to the crustal character of all of these rocks.

A fairly important factor in the identification of genetic links between the magmatic rocks is the similar crystallization sequences of the magmas of the Chineiskii and Mailavskii massifs and the Main Dike at the Udokan deposit (Fig. 14, Table 10). The modeled crystallization sequences of minerals in these rocks are close to the aforementioned "magnesian" evolutionary trend of the Chineiskii magmas. It is important to emphasize that these sequences begin with the crystallization of olivine, which disappears due to a peritectic reaction with the melt at decreasing temperature. In this context, the closest similarities are exhibited by the titanomagnetite-bearing gabbro of the Mailavskii Massif and the most primitive of the recognized petrochemical

Table 9. Composition of rocks from the Chineiskii Complex

Component	1	2	3	4
	9	5008	5068	9401
SiO_2	52.75	47.3	54.77	52.11
TiO_2	0.84	1.97	0.77	0.65
Al_2O_3	16.32	9.27	14.27	15.41
FeO	11.35	17.16	11.7	11.99
MnO	0.17	0.18	0.16	0.17
MgO	7.59	8.28	4.99	7.42
CaO	7.63	13.65	9.41	8.99
Na_2O	2.63	1.69	2.66	2.74
K_2O	0.65	0.4	1.2	0.96
LOI	0.07	0.08	0.1	0.11
Total	100	99.98	100.03	100.55
Cs	–	0.496	1.121	0.987
Rb	–	22.8	40.3	35.0
Ba	–	220.0	466.7	395.1
Th	–	1.917	4.757	4.505
U	–	0.596	1.244	0.963
Nb	–	2.407	5.616	6.199
Ta	–	0.198	0.544	0.463
La	–	8.384	19.852	16.609
Ce	–	18.3	41.2	34.7
Pr	–	2.345	4.847	4.052
Sr	–	228.8	261.0	287.8
Nd	–	9.685	18.772	16.064
Sm	–	2.162	3.789	3.202
Zr	–	43.956	97.310	97.023
Hf	–	1.151	2.598	2.315
Ti	–	12392.1	4895.1	4010.9
Eu	–	0.695	1.298	1.038
Gd	–	2.156	3.458	3.141
Tb	–	0.345	0.547	0.489
Dy	–	2.135	3.347	2.937
Y	–	13.2	20.2	19.7
Ho	–	0.445	0.711	0.621
Er	–	1.237	2.016	1.741
Tm	–	0.181	0.299	0.266
Yb	–	1.127	1.885	1.704
Lu	–	0.167	0.284	0.259

Note: Samples: 9—petrochemical type in Table 3 (gabbronorite); 5008—titanomagnetite-bearing leucogabbro form the Mailavskii Massif; 5068 and 9401—Main Dike of the Udokan deposit (gabbronorite).

rock types: the titanomagnetite magmas of the Chineiskii pluton (type 9). In the former instance, relatively magnesian olivine (Fo_{76}) appears on the liquidus. The composition of olivine in the latter case corresponds to Fo_{85}. Both compositions are characterized by the subcotectic crystallization of augite, plagioclase, and magnetite within a narrow temperature range (15–20°C).

The crystallization sequence of the rocks composing the Main Dike at the Udokan deposit (sample 9401) is similar to this sequence: it also begins with the crystallization of olivine (of the composition Fo_{81}), but plagioclase appears there earlier than augite, and magnetite crystallizes concurrently with low-Ca pyroxene. More significant differences were detected for the phase relations of another dike (sample 5068), whose crystallization began with a plagioclase–clinopyroxene cotectic, which was followed by the appearance of magnetite. More detailed conclusions require additional studies based on more representative material.

The most complicated problem is presented by the genesis of the Chineisskii Massif itself. This follows, first of all, from geological data: the heterogeneity of the inner structure of the intrusion, the unsystematic localization of certain rock groups in its vertical section, variations in the thicknesses of certain units (up to their pinching out and complete disappearance), and the occasional occurrence of magmatic contacts between rocks. As was mentioned above, discrete blocks of the massif differ in inner structure due to the compositional specifics of the rocks and their layering and rhythmicity. Undoubtedly, the morphology and composition of the rocks of group I (first of all, the pyroxenites) testify that they were entrained in the form of xenoliths of variable size during the emplacement of the bulk of the magma. Also, the younger age of the fourth rock group (lamprophyres) does not provoke any doubt, because the setting of these rocks is controlled by an array of nearly horizontal faults at the boundary of the bottom of the gabbroids and sandstones of the Udokan Complex.

Another very complicated problem is the genesis of the bulk of the massif. Given the aforementioned features of the inner structure of the massif as a whole and its vertical section, the relations and genesis of its rocks of the second and third groups can be interpreted from various viewpoints.

From one of them, the origin of contrasting structural–phase boundaries between the rocks can be explained by a single major pulse (in the geological sense, a single act of melt emplacement) of genetically interrelated but slightly differentiated magmas of similar temperature that were variably enriched in intratelluric phenocrysts of various minerals. The residual melts were then intruded into the already crystalline rocks. An illustration of this mechanism may be the independent emplacement of residual melts in large plutons (so-called autointrusions), which are com-

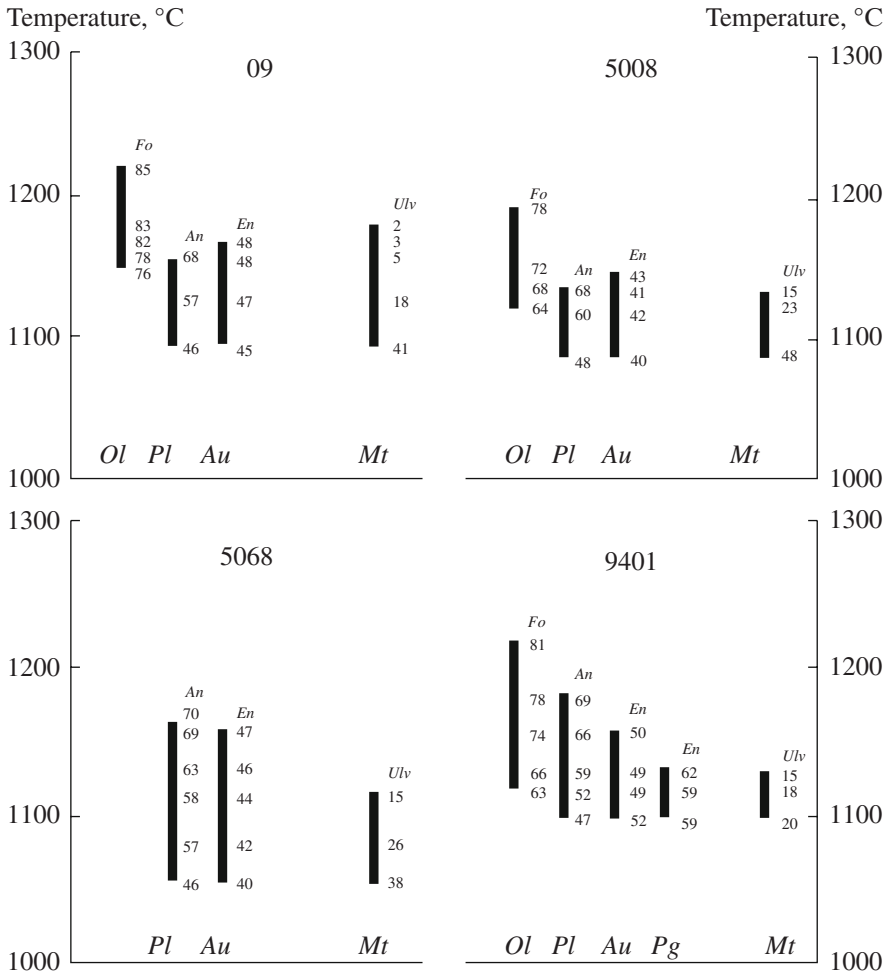

Fig. 14. Temperatures and crystallization sequences of primitive rocks from the Chineiskii Massif (type 9), the Mailavskii intrusion (sample 5008), and dikes of the Udokan deposit (samples 5068, 9401). Mineral symbols are the same as in the note to Table 5.

monly unambiguously identified during fieldwork based on the structural-phase differences from most of the host rocks.

At the same time, it may be hypothesized that the initial melt was during its emplacement in equilibrium with abundant and unevenly distributed crystalline

Table 10. Weighted average composition of rocks from the Chineiskii Massif, wt %

No.	Number of analyses	SiO_2	TiO_2	Al_2O_3	Fe_2O_3	MnO	MgO	CaO	Na_2O	K_2O	P_2O_5	LOI	Total
1	987	44.81	2.38	14.26	20.41	0.17	5.95	8.53	2.32	0.66	0.07	0.25	99.81
2	16	49.78	1.12	13.43	14.71	0.20	9.31	8.00	2.52	0.83	0.07	0.67	100.62
3	31	43.20	2.61	14.11	21.32	0.17	5.72	9.42	2.72	0.73	0.05	0.44	100.49
4	20	44.65	2.29	14.22	17.95	0.17	6.09	11.10	3.06	0.54	0.08	0.25	100.40
5	85	44.20	2.38	14.37	19.71	0.17	6.18	9.34	2.84	0.68	0.07	0.45	100.38
6	2	44.41	2.14	14.58	19.42	0.2	6.2	10.12	2.4	0.31	0.08	0.17	100.03
7	2	47.57	1.15	15.4	12.72	0.14	6.54	7.68	1.44	2.57	0.23	3.70	99.14

Note: (1) Arithmetic mean for the massif; (2–7) weighted average compositions: (2) gabbronorite series, (3) titanomagnetite gabbro series, (4) leucogabbro series, (5) section through Hole 83, (6) cement of the magmatic breccias, (7) cement of the fluid–magmatic breccias.

Fig. 15. Distribution of concentrations of Ti and trace elements normalized to the primitive mantle composition [42] for monzodiorites (0305, Table 8), gabbronorites from the Main Dike of the Udokan deposit (9401, 5068, Table 9), Lukturskii Massif (0308, Table 8), gabbrodiorites (0304), and titanomagnetite gabbro (0306) from the Chineiskii Massif (Table 8) and titanomagnetite gabbro from the Mailavskii Massif (Table 9).

phases (olivine, plagioclase, and magnetite) when still in the magmatic reservoir, before the emplacement of the magma into the modern intrusion chamber.

We also hold for the latter opinion. Sharp contacts between the rocks of groups II and III testify that the magmas were emplaced successively (with time spans separating discrete emplacements), had different compositions, and were rich in different intercumulus minerals. This is largely confirmed by rock relations opposite to those described above: observations suggest not the emplacement of residual melts but their reversed (from acid to basic) compositional trend with time, with the youngest melts (norites of the third group) being the most primitive magmas compared to their host rocks of the second group (titanomagnetite gabbro, gabbronorites, and leucogabbro). The absence of a systematic evolution of the cumulus mineral assemblages in the vertical section of the intrusion also confirms this conclusion.

Hence, we believe that our simulation results suggest that the rocks of all four rock groups of the massif were derivatives of a single parental magma, which initially contained a "mush" of olivine, plagioclase, and magnetite crystals at a temperature of approximately 1130°C. The gravitational separation of these phases before the emplacement of the magma into a chamber and the relative migration of the magmatic suspensions of various phase composition, the long-lasting and simultaneous character of the emplacement of the magmas, could give rise to an uneven distribution of the solid phases in the volume, and this, in turn, is now reflected in the heterogeneity of the mineralogical composition of the rocks composing the massif. Consequently, discrete melt portions produced by the evolution of the initial magma gave rise to different "parental" magmas of rocks in the discrete blocks. The first magma portion to be emplaced was leucocratic (it carried plagioclase and titanomagnetite as the predominant solid phases) and was intruded into the western and southwestern blocks. Later, already in the chamber, the magma underwent differentiation, which produced small- and large-scale banding. A possible mechanism responsible for its development was proposed in [49]. It was thereby hypothesized that the 80% crystalline melt acquired characteristics of a Newtonian liquid in which solidification shrinkage cracks could form; the latter could be filled with residual anorthosite melt, a fractionation product of the melts of the titanomagnetite gabbro (TMG) series.

During the next evolutionary stage of the massif, magma portions enriched in orthopyroxene and plagioclase were emplaced into various parts of the chamber. Its crystallization produced the rocks of the norite series, which are predominant in the central part of the intrusion.

The relative role of the crystallization differentiation of the Chineiskii magmas in the chamber remains uncertain within the scope of the scheme proposed above and requires further studying.

The composition of the rocks of the Chineiskii Complex is compared to those of the rocks of the Upper Zone of the Bushveld pluton. The latter are the closest to the rocks of the Lukturskii Massif, whose data points plot practically exactly onto the compositional trend of this zone in the Bushveld Massif (Fig. 16). Table 9 presents the average composition of the Chineiskii intru-

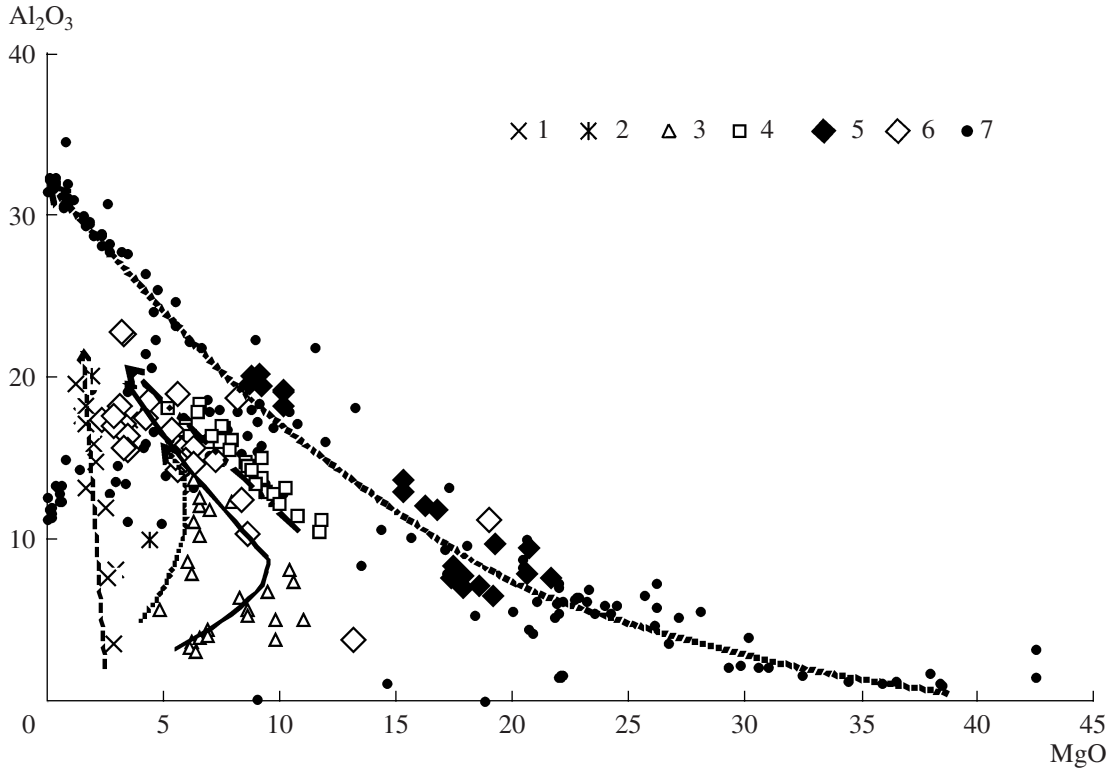

Fig. 16. MgO–Al_2O_3 diagram for rocks from (1–4) the Chineiskii, (5) Lukturskii, (6) Mailavskii (6), and (7) Bushveld massifs: (1) chinite, (2) titanomagnetite-bearing gabbro from the depth interval of 560–562 m, Hole 11, (3) gabbroids from microrhythms 110622, 110642, and 110620, (4) rocks of the norite series.

sion as a whole, the weighted average composition of its discrete series, and the weighted average composition of the rocks documented in the reference vertical section. The calculated composition of the modeled melt (Table 7) is the closest to the weighted average composition of the gabbronorite series.

CONCLUSIONS

(1) The results of geological–geophysical observations, geochemical features of the ultrabasic–basic rocks of the Kodar–Udokan district, and petrological reconstructions led us to the conclusion that the Chineiskii intrusion, which is exposed at the modern erosion surface in the form of a magmatic body of complex structure, is merely a small portion of a large Paleoproterozoic magma-conducting system (namely, its deepest part, along with the Lukturskii and Maislavskii massifs). The subvolcanic rocks composing this system also include a number of tabular bodies (the Main Dike of Udokan and dikes intruding the host rocks of the Chineiskii Massif).

(2) The Chineiskki Massif is thought to have been produced by successive emplacement of magmas, which formed four rock groups. These are the pyroxenite of the second group (which now occur in the form of xenoliths), titanomagnetite gabbronorites and leucogabbro of the second group, gabbronorites of the third group, and lamprophyres of the fourth group (which compose small dikes and tabular bodies in the bottom part of the intrusion).

(3) The trace-element patterns of various rocks and the results of simulations by the COMAGMAT-3.5 computer program led us to believe that all four rock groups of the massif were generated by the successive emplacements of several portions of the initial magma, which was a complicatedly differentiated suspension of olivine, plagioclase, and magnetite crystals in ferroabsaltic melt at a temperature of approximately 1130°C.

(4) The gravitational separation of these phases in the melt before its emplacement into the chamber and during the subsequent emplacement of various portions of the initial magma into the modern chamber predetermined the heterogeneity of the massif (its block structure). As a result, the bulk of the Chineiskii Massif is composed of compositionally principally different rocks of the second and third groups, with the predominance of intratelluric plagioclase and magnetite crystals in the former case (gabbronorite and leucogabbro series in the western and southeastern blocks) and orthopyroxene in the latter one (norite series, central block). The rocks of the third group were generated later.

(5) The crystallization sequences of minerals modeled for the Chineiskii Massif can be classed into two

major types: (a) "high-Al", which is typical of the "leucogabbro" compositions and characterized by the occurrence of a magnetite–plagioclase cotectic, and (b) "high-Mg", which is typical of the noriteseries and is characterized by the early appearance of olivine on the liquidus or the concurrent crystallization of this mineral with magnetite or plagioclase.

(6) It is worth mentioning the early appearance of *Ol-Mt* and *Ol-Pl* on the liquidus and the cotectic crystallization of these minerals in the rocks of the Chineiskii and Mailavinskii massifs and in the gabbroids of the Udokan Dike, which highlights genetic links between them. The crystallization sequences of the minerals demonstrate that olivine was in reaction relations with the melt, completely dissolved due to a peritectic reaction at temperatures of $T = 1110–1150°C$, and was replaced (completely or partly) by pyroxenes and magnetite. These data testify that the initial melts were saturated or slightly oversaturated with SiO_2 and that the intercumulus systems had elevated SiO_2 concentrations.

ACKNOWLEDGMENTS

This study was supported by the Russian Foundation for Basic Research, project no. 07-05-01007.

REFERENCES

1. L. R. Wager and G. M. Deer, *Layered Igneous Rocks* (Oliver and Boyd, Edinburgh–London, 1939).
2. L. R. Wager and G. M. Braun, *Layered Igneous Rocks* (Mir, Moscow, 1970) [in Russian].
3. A. A. Yaroshevskii, "Origin of Rhythmic Structures of Igneous Rocks," Geokhimiya, No. 5, 562–574 (1970).
4. E. V. Sharkov, *Genesis of Layered Intrusions and Related Mineralization* (Nauchnyi Mir, Moscow, 2006) [in Russian].
5. H. V. Eales and R. G. Cawthorn, "The Bushveld Complex," in *Layered Intrusions,* Ed. by R. G. Cawthorn (Elsevier, Amsterdam, 1996), pp. 181–230.
6. A. F. Grachev, *Problems of Global Geodynamics* (GEOS, Moscow, 2000) [in Russian].
7. K. C. Condie, *Mantle Plumes and Their Record in Earth History* (University Press, Cambridge, 2001).
8. *Geological Structure and Mineral Resources of the Chita Segment of BAM: Analytical Review* (Chita, 2002) [in Russian].
9. A. I. Kulikov, V. K. Golev, V. M. Grigor'ev, and V. K. Kryukov, "Geological Structure and Titanomagnetite Ores of the Chinei Gabbroid Massif," in *Geology and Exploration of Mineral Deposits* (Irkutsk, 1981), pp. 26–35 [in Russian].
10. N. A. Krivolutskaya, "Sulfide Mineralization of the Chinei Massif," Geol. Rudn. Mestorozhd., No. 5, 94–100 (1986).
11. B. I. Gongal'skii, N. A. Krivolutskaya, and N. G. Goleva, "Mineral Deposits of the Chinei Massif," in *Mineral Deposits in Transbaiklia* (Geoinformmark, Moscow, 1995), Vol. 1, No. 1, pp. 20–28 [in Russian].
12. B. I. Gongal'skii, A. E. Izokh, A. P. Krivenko, et al., "Giant Copper Accumulation in Mineral Deposits of the Kodar–Udokan Region (Northern Transbaikali)," in *Large and Superlarge Deposits: Genesis and Localization* (IGEM, Moscow, 2004), pp. 206–218 [in Russian].
13. B.I. Gongalsky and N.A. Krivolutskaya, "Unique Copper Metallogenic Province of the North Transbaikalia (Siberia, Russia)," in metallogeny of the Pacific Northwest: Tectonic, Magmatism and metallogeny of Active Continental Margius (Vladivostok, Dalnauka, 2004), pp. 443–446.
14. N. D. Tolstykh, A. P. Krivenko, N. A. Krivolutskaya, et al., "Noble Metal Mineralization of Sulfide Ores of the Chinei Pluton," in *Platinum of Russia (Geoinformmark, Moscow, 2004),* Vol. 5, pp. 225–250 [in Russian].
15. D. A. Dodin, *Metallogeny of the Taimyr–Norilsk Region, Northern Central Siberia* (Nauka, St. Petersburg, 2002) [in Russian].
16. M. N. Petrusevich, "Chinei Titanomagnetite Deposit," Sov. Geol., No. 10, 91–94 (1946).
17. N. B. Belova, Extended Abstracts of Candidate's Dissertation in Geology and Mineralogy (MGRI, Moscow, 1980) [in Russian].
18. E. G. Konnikov, *Differentiated Ultrabasic–Basic Precambrian Complexes in Transbaikalia* (Nauka, Novosibirsk, 1986) [in Russian].
19. A. V. Tatarinov, L. I. Yalovik, and V. S. Chechetkin, *Dynamometamorphic Model for the Genesis of Layered Mafic Rock Massifs as Exemplified by the Chinei Massif in Northern Transbaikalia* (Nauka, Novosibirsk, 1998) [in Russian].
20. V. V. Arkhangel'skaya, Yu. V. Bykov, R. N. Volodin, et al., *Udokan Copper and Katugin Rare-Metal Deposit of the Chita District, Russia* (Chita, 2004) [in Russian].
21. V. E. Khain, *Tectonics of Continents and Oceans* (Nauchnyi Mir, Moscow, 2000) [in Russian].
22. F. M. Stupak, *Cenozoic Volcanism of the Udokan Range* (Nauka, Novosibirsk, 1987) [in Russian].
23. Yu. V. Zorin, E. Kh. Turutanov, M. R. Novoselova, and T. Balk, "Volume Model of the Lithosphere of the Southern Part of Eastern Siberia," Geotektonika, No. 1, 96–106 (1989).
24. A. P. Birkis and L. I. Koshik, *Anorthosites of the Earth and Moon* (Nauka, Moscow, 1984) [in Russian].
25. B. I. Gongal'skii, A. S. Golovatyi, and S. A. Abushkevich, "Zoned Ring Structures of the Udokan Range," Dokl. Akad. Nauk **343** (1), 80–82 (1995).
26. F. P. Krendelev, N. N. Bakun, and R. N. Volodin, *Cupriferous Sandstones of Udokan* (Nauka, Moscow, 1983) [in Russian].
27. A. M. Larin, A. B. Kotov, E. B. Sal'nikova, et al., "New Data on the Age of Granites of the Kodar and Tukuringra Complexes, Eastern Siberia: Geodynamic Constraints," Petrologiya **8** (3), 267–279 (2000) [Petrology, 238–248 (2000)].
28. "Geological Structure of the USSR and Tendencies in the Distribution of Mineral Resources," in *The Altai–Sayan and Transbaikalia–Upper Amur Region. Transbaikalia–Upper Amur Region*, Ed. by V. D. Amantova (Nedra, Leningrad, 1986), Vol. 7, Book 2 [in Russian].

29. A. P. Lebedev, *Chinei Gabbro–Anorthosite Pluton* (East Siberian) (Moscow, 1962) [in Russian].
30. A. J. Naldrett, *Magmatic Sulfide Copper–Nickel and PGE Deposits* (SPbGU, St. Petersburg, 2003) [in Russian].
31. B. I. Gongal'skii, *Atlas of the Rock Relation in the Chinei Layered Pluton, Northern Transbaikalia* (ChIPR SO AN SSSR, Chita, 1990) [in Russian].
32. B. I. Gongal'skii and N. A. Krivolutskaya, *Chinei Layered Pluton* (Nauka, Novosibirsk, 1993) [in Russian].
33. K. M. Mel'nikova, V. K. Kryukov, N. B. Belova, et al., "Localization of Mineralization in the Chinei Layered Basic Massif, Udokan Ore District," in *Endogenous Processes and Metallogeny in the BAM Region* (Nauka, Novosibirsk, 1983), Vol. 2, pp. 25–30 [in Russian].
34. B. I. Gongal'skii, "Place of Chinites (Plagioclase–Titanomagnetite Rocks) in the Formation of the Chinei Layered Pluton," Byull. Mosk. O-va Ispyt. Prir., Otd. Geol. **68** (2), 83–88 (1993).
35. B. I. Gongal'skii and N. A. Krivolutskaya, "Microrhythm 1106420 of the Chinei Pluton," Dokl. Akad. Nauk SSSR **296** (5), 1199–1203 (1987).
36. A. A. Yaroshevskii, "Geochemical Structure of Magmatic Complexes: An Example of the Kivakka Layered Olivinite–Norite–Gabbronorite Intrusion, Northern Karelia," Geokhimiya, No. 12, 1251–1270 (2004) [Geochem. Int. **42**, 1107–1125 (2004)].
37. A. A. Yaroshevskii, S. V. Bolikhovskaya, and E. V. Koptev-Dvornikov, "Geochemical Structure of the Yoko-Dovyren Layered Dunite–Troctolite–Gabbro–Norite Massif, Northern Baikal Area," Geokhimiya, No. 10, 1027–1039 (2006) [Geochem. Int. **44**, 953–964 (2006)].
38. J. H. Ward, "Hierarchical Grouping to Optimize an Objective Function," J. Amer. Stat. Assoc **58** (301), 236–244 (1963).
39. G. S. Barmina, A. A. Ariskin, and M. Ya. Frenkel, "Petrochemical Types and Crystallization Conditions of Plagiodolerites of the Kronotsky Peninsula, Eastern Kamchatka," Geokhimiya, No. 2, 192–206 (1989).
40. A. A. Ariskin and G. S. Barmina, *Modeling of Phase Equilibria during the Crystallization of Basaltic Magmas* (Nauka, MAIK "Nauka/Interperiodika", Moscow, 2000) [in Russian].
41. A. A. Ariskin and G. S. Barmina, "COMAGMAT: Development of Magma Crystallization Model and Its Petrological Applications," Geochem. Int. **42** (Suppl. 1), 1–157 (2004).
42. A. W. Hofmann, "Chemical Differentiation of the Earth: Relationship between Mantle, Continental Crust, and Oceanic Crust," Earth Planet. Sci. Lett. **90**, 297–314 (1988).
43. J. L. Joron and M. Treuil, Hydromagmafile Element Distributions in Oceanic Basalts as Finger of Partial Melting and Mantle Heterogeneities: A Specific Approach and Proposal of an Identification and Modeling Method, in *Magmatism in Ocean Basins* Geol. Soc. Spec. Publ. **42**, 277–299 (1988).
44. A. W. Hofmann, "Sampling Mantle Heterogeneity through Oceanic Basalts: Isotopes and Trace Elements," Treatise on Geochemistry **2**, 61–101 (2003).
45. O. A. Bogatikov, V. I. Kovalenko, E. V. Sharkov, and V. V. Yarmolyuk, *Magmatism and Geodynamics. Terrestrial Magmatism throughout the Earth's History* (Gordon and Breach Science Publishers, Amsterdam, 2000).
46. E. V. Sharkov, O. A. Bogatikov, V. F. Smol'kin, et al., "Origin of Large Layered Intrusions: Evidence from Early Proterozoic Large Igneous Province of Siliceous High-Magnesian Series," in *Mantle Plumes and Metallogeny* (Moskva, Petrozavodsk, 2002), pp. 281–284 [in Russian].
47. T. T. Allapieti and J. J. Lahtinen, "Platinum-Group Element Mineralization in Layered Intrusions of Northern Finland and Kola Peninsula, Russia," in *The Geology, Geochemistry and Mineral Beneficiation of Platinum-Group Elements*, Ed by J. Cabri, Canad. Inst. Mining Metallurgy, Spec. **54**, 507–546 (2002).
48. A. N. Wilson, "The Great Dyke of Zimbabwe," in *Layered Intrusions*, Ed. by R. G. Cawthorn (Elsevier, Amsterdam, 1996), pp. 181–230.
49. N. L. Dobretsov, E. G. Konnikov, and L. A. Tsoi, "New Model of the Formation of Rhythmical Layering of the Basic Plutons," Geol. Geofiz., No. 2, 3–11 (1984).